Chapter 7
Multijunction Approaches to Photoelectrochemical Water Splitting

Eric L. Miller, Alex DeAngelis, and Stewart Mallory

7.1 Introduction

Hydrogen is an extremely valuable chemical commodity, not only in today's industrial marketplace, but even more so in the emerging *Green Economies* so vital to the future of our planet and its people. *Green* futures will need to rely less-and-less on fossil fuels, and more-and-more on solar, wind, biomass, geothermal, and other renewable energy resources. Hydrogen is envisioned as one of the primary media for the storage and distribution of energy derived from this renewable portfolio. To achieve the vision, much work is needed in the development of new more practical technologies and infrastructures for hydrogen production, storage, delivery, and utilization. Nonpolluting technologies for large-scale hydrogen-production utilizing renewable energy are of particular importance.

Among the viable renewable hydrogen-production approaches, solar options, particularly solar-powered water-splitting, offer the best hope for large-scale renewable production with low carbon emissions. Several solar-to-hydrogen (STH) pathways are possible, including solar electrolysis, where electricity generated by photovoltaic (PV) or concentrated solar thermal (CST) power plants is used to drive electrolyzer systems, for example, commercial "alkaline" or "PEM" electrolyzers. Among a number of alternative, more direct conversion pathways, photoelectrochemical (PEC) water-splitting using semiconductor photoelectrodes or photocatalysts remains one of the most promising, though still elusive based on challenges in developing stable and efficient PEC materials, devices, and systems. Broadly speaking, a PEC system combines the harnessing of solar energy and the electrolysis of water into a single conversion system. As illustrated in Fig. 7.1,

E.L. Miller (✉)
U.S. Department of Energy, Washington, DC, USA
e-mail: eric.miller@hq.doe.gov

A. DeAngelis • S. Mallory
University of Hawaii at Manoa, Honoulu, HI, USA

R. van de Krol and M. Grätzel (eds.), *Photoelectrochemical Hydrogen Production*, Electronic Materials: Science & Technology 102, DOI 10.1007/978-1-4614-1380-6_7,

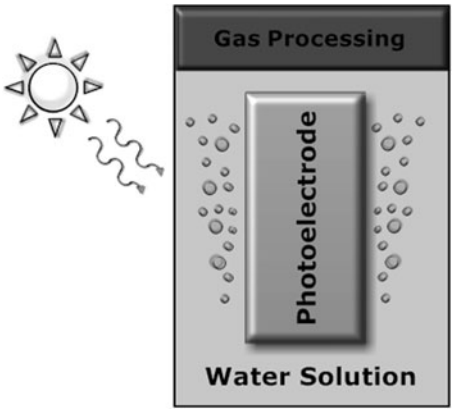

Fig. 7.1 A PEC photosensitive electrode uses sunlight to split water, evolving hydrogen and oxygen gases from solution

sunlight shining on a suitable PEC semiconductor device immersed in a water-based solution can simultaneously drive water oxidation and hydrogen reduction electrochemical reactions to split water. This process evolves hydrogen and oxygen gases, effectively converting the solar energy in to stored chemical energy.

The PEC approach is simple and elegant in concept, but is challenging to implement in practice since it relies on complex interactions involving sunlight, semiconductors, and liquid solutions. In a practical system, the semiconductor material must efficiently absorb sunlight and generate sufficient photovoltage to split water, while the semiconductor interface must be favorable to sustaining the hydrogen- and oxygen-gas evolution reactions. In addition, the PEC system needs to remain stable in solution, and must be inexpensive for compatibility with large-scale deployment. To date, no known semiconductor system achieves *all of the above criteria* – though some have come close. PEC devices based on multijunction III–V semiconductor technology have been demonstrated at the National Renewable Energy Laboratory (NREL) with impressive STH conversion efficiencies (i.e., the ratio of the chemical energy available in the generated hydrogen to the incident solar energy) exceeding 12% [1–4]. Unfortunately, these III–V devices have lacked long-term stability, and moreover, they utilize a number of prohibitively expensive materials as seen in the multilayered device structure illustrated in Fig. 7.2. Lower cost PEC devices based on thin-film semiconductors, also in multijunction configurations, have demonstrated stable hydrogen conversion efficiencies ranging from 3 to 8% [5–8], but progress toward higher performance in such devices has been slow. Before practical PEC hydrogen production can become a reality, key scientific advancements in the development of new PEC materials and devices are still needed.

Toward this end, the most advanced scientific techniques in materials theory, synthesis, and characterization are being brought to the table on an international scale, and powerful synergies among researchers in the PEC, photovoltaics, and nanotechnology fields are emerging in collaborative pursuit of the PEC *quest* [9].

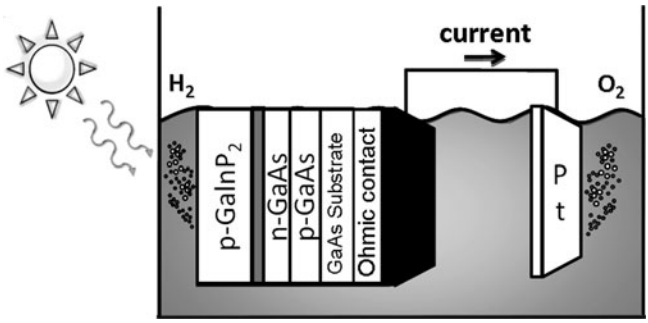

Fig. 7.2 Illustration of multilayered III–V semiconductor device structure that has demonstrated high solar-to-hydrogen conversion efficiencies for limited durations

In fact, PEC researchers often stake claim to PEC as the *Holy Grail of hydrogen production* [10, 11]. This may seem somewhat overly dramatic, though PEC is unique in offering an efficient low-cost approach for harnessing solar energy to produce high-purity hydrogen from water, at low operating temperatures, with no carbon emissions. The key to successful deployment will be in the identification and development of innovative materials systems, likely involving multijunction semiconductor configurations similar to that seen in Fig. 7.2.

Multijunction approaches offer some of the best hope for achieving practical PEC hydrogen production in the near term, but complicated materials and interface issues need to be addressed by the scientific community. This chapter explores the challenges and benefits of large-scale solar water splitting for renewable hydrogen production, with specific focus on the multijunction PEC production pathways. The technical motivation and approach in the R&D of multijunction PEC devices are considered, and examples of progress in laboratory scale prototypes are presented.

7.2 Solar-to-Hydrogen Conversion

Hydrogen is a valuable chemical commodity. Today, it is a vital component in the industrial processing of important chemical commodities, such as fuels and fertilizers. In the near future, it could take on new significance as a viable alternative to gasoline or electricity as an energy carrier for stationary power and transportation applications. On a commercial scale, STH conversion, specifically in the form of solar water-splitting, offers the best hope for *renewable* production with low carbon emissions. This approach for large-scale industrial deployment is truly *renewable* and *sustainable* considering the enormity of the solar resource and the abundance of water as a low-cost feedstock for hydrogen production. The "re-cycling" of water as a by-product of hydrogen fuel cell and combustion utilization schemes also factors into the *sustainability* of solar water splitting.

7.2.1 Value of Hydrogen

Hydrogen has become a hot topic in recent years, both in political and scientific circles. A national spotlight was cast on hydrogen in Former President George W. Bush's State of the Union Speech in 2004, which featured such memorable quotes as: "America can lead the world in developing clean, hydrogen powered automobiles" and "With a new national commitment, our scientists and engineers will overcome obstacles to taking these cars from laboratory to showroom" [12]. Similar optimism has been expressed across the board by politicians, economists, and scientists, as exemplified in Jeremy Rifkin's canonical work "The Hydrogen Economy" [13]. Still, there is by no means universal acceptance. From the opposing perspective, energy expert Joseph J. Romm in his book *The Hype About Hydrogen* asserts: "Neither government policy nor business investment should be based on the belief that hydrogen cars will have meaningful commercial success in the near- or medium-term" [14].

Whatever view you take on the future importance of hydrogen in our society, the world's most abundant element is in fact an extremely valuable chemical commodity today. In the contemporary industrial marketplace, hydrogen is a high volume chemical with US production exceeding 20 billion kg annually [15]. Important industry uses include the production of chemicals, processing of materials, semiconductor manufacturing, generator cooling, and fertilizer production. In fact, the demand for hydrogen has been expanding significantly in recent years, especially in the fuels processing sector. As petroleum crude becomes dirtier, and as biomass feedstocks enter the fuels mix, growing amounts of hydrogen are being required for "hydrocracking" in the refining processes [16].

Hydrogen's low density, high thermal conductivity, and strong chemical reducing properties make it ideal for the broad ranging industrial applications discussed above. To satisfy the expanding demand, current hydrogen production continues to rely primarily on established fossil-fuel technologies. Worldwide, over 95% of hydrogen is produced from natural gas, oil, or coal, with production relying largely on steam-methane reforming (SMR) with downstream purification processes such as pressure swing absorption (PSA) [17]. Of course, fossil fuels are vulnerable to dwindling availability and rising cost, and result in carbon emissions and other forms of environmental contamination. The current fossil-based industries for hydrogen production and utilization still suffer the risks and disadvantages of our current *Fossil Fuel Economy*. New, cleaner, and long-term approaches to hydrogen production and utilization are essential, not only to sustain current levels of demand, but also to accommodate future expanded *Hydrogen Economy* markets [13, 18–20].

In visions of a future *Hydrogen Economy*, hydrogen is an ideal energy carrier for the storage and distribution of renewable energy resources such as solar, wind, geothermal, and hydroelectric. Using fuel-cell or combustion engine technologies, hydrogen can be converted simply and cleanly to power or heat with no carbon emissions, and with water as the primary by-product. Unfortunately, although hydrogen is nature's most abundant element, it exists primarily in strongly bonded chemical compounds, and extracting it involves difficult and energy-intensive processes. With current technologies, production, storage, and utilization of this

ideal energy carrier are all challenging. An enormous amount of technology and infrastructure development would be needed to attain a pure *Hydrogen Economy*. More realistically, a *Green Economy* will emerge comprising a broad portfolio of alternative energy sources and carriers, including hydrogen. As our present reliance on petroleum-based fossil fuels become increasingly difficult to sustain, both economically and environmentally, this will become inevitable. As a result, new, more distributed approaches to national and world energy management will take hold. Different locations rich in their own renewable resources will manufacture energy currencies such as electricity or hydrogen for large-scale distribution to the broader energy marketplace. Electricity is a key energy carrier today, and will remain so long into the future. Hydrogen, however, will also emerge in an important complementary role, providing important benefits in large-scale energy storage and long-distance distribution.

Hydrogen is indisputably valuable today, and will become increasingly valuable as an energy carrier with the future development of new renewable energy production and distribution infrastructures. In the process, new and improved technologies will emerge for the economical and environmentally friendly production, storage, delivery, and utilization of hydrogen. Production technologies using solar energy to split water are enormously attractive, motivating accelerated PEC research and development. Current research in multijunction PEC devices will be particularly important to near-term deployment of large-scale solar hydrogen production, as discussed in the following sections.

7.2.2 The Solar Resource

The true value of the solar resource as a renewable energy commodity becomes painfully apparent considering the current situation of oil. According to the US Energy Information Administration (EIA), the current worldwide oil in reserves totals approximately 213 trillion liters [21]. The amount of oil consumed globally as of 2008 was determined to be 5 trillion liters [22]. The projected oil consumption growth rate between 2004 and 2030 is expected to be approximately 1.6% [23]. Figure 7.3 shows projected oil consumption in relation to known oil reserves, both at current consumption levels and for a projected growth of 1.6% per year. As can be seen, even if the current consumption does not increase, the current oil reserves will become significantly depleted over the next 50 years.

New oil reserves will be found, yet the fact remains that this is a shell game of diminishing returns. Oil is a finite commodity, and before it runs out entirely, it will become increasingly energy-intensive and costly to extract from the earth and process into fuels. Creating a renewable alternative to satisfy our world's energy appetite is likely to be the challenge of our Age. As Dr. Carl Safina aptly noted: "Whoever owns the new sources of energy will own the future economy" [24].

Our best hope for the future is the sun, the ultimate renewable energy resource, continuously bombarding Earth with about 180,000 TW of radiant power. This is enough to power about 10 quadrillion compact fluorescent light bulbs; over

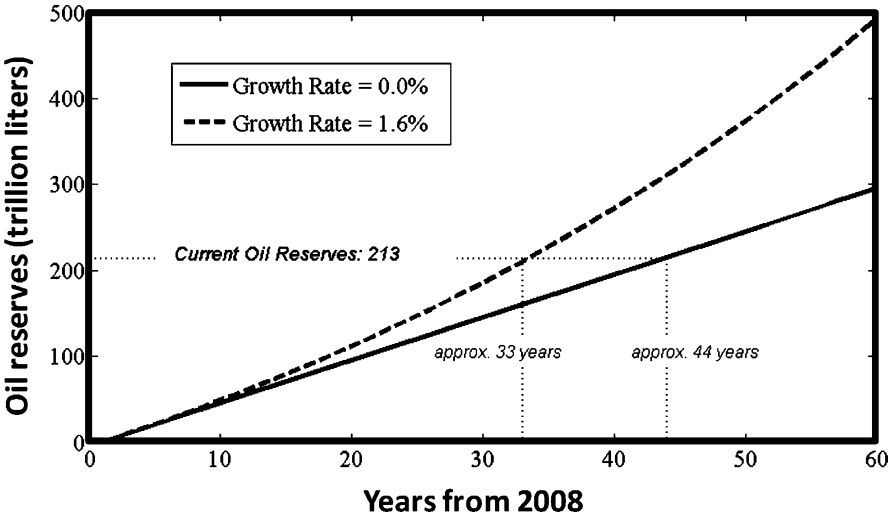

Fig. 7.3 Projected exponential growth of oil consumption plotted for 0.0 and 1.6% growth rates given current global oil reserves

10 million bulbs for every person on the planet! [25, 26]. Approximately 36,000 TW of the incident solar power strikes earth's land masses where terrestrial-based solar-energy conversion plants could be constructed. To put this in perspective, our society on average consumes 13–15 TW, with projected increases up to 30 TW over the next 50 years, consistent with trend shown in Fig. 7.3 [27]. These energy consumption numbers are enormous, but still represent a small fraction of the sun's influx of radiant power. Of course, the planet relies on the sun for many things, including sustaining plant-life and driving its weather patterns, so not all of the incident solar energy is available for mankind's energy hunger. Still there is significant solar energy to spare. Using 10% solar energy conversion systems, 30 TW could be produced using only 0.25% of the land.

Unfortunately, it is not that easy. The large-scale conversion of solar energy to mechanical work or electricity is currently quite challenging and costly. At peak times of daylight, the solar intensity available for terrestrial conversion scales to approximately 1,000 W/m^2. Large collection areas and significant landmass would therefore be needed for commercial scale power production. Such expansive commercial deployment requires an enormous capital investment. For example, commercial photovoltaic technologies today can convert sunlight to electricity at efficiencies between 10 and 20%, at $2–5 per installed Watt [28]. A single Gigawatt plant would cost billions of dollars and span over 2,500 acres. As an added disadvantage, these expensive behemoths would be inoperative at nighttime and ineffectual under any significant cloud coverage.

There are practical difficulties and challenges, but the sun is still the most promising of renewable resources, and the most underutilized in modern society. Currently, less than 0.1% of the world energy production is from solar energy

plants, though this number is starting to increase [29]. Encouragingly, improved technologies for solar energy conversion, storage, and utilization are emerging to make their impact on the world energy scene. New and improved solar-to-electric and STH conversion technologies are all poised to be part of the new energy mix. Developing the most practical and efficient technologies to convert sunlight to useable energy carriers such as electricity or hydrogen is a critical priority. With its potential benefits, PEC hydrogen production remains an attractive conversion route for large-scale solar hydrogen production.

7.2.3 Solar Conversion Pathways

In converting sunlight, whether to electricity or to hydrogen, fundamental thermodynamic principles govern the energy conversion process. The sun radiates energy at a *black body temperature* of 5,780 K, while the Earth's black body temperature is 300 K. The Carnot limit between these source and sink temperatures is readily calculated as 95%, representing the amount of radiant energy can be converted into other more useable energy forms [30]. Though this is encouraging, actual conversion of sunlight to practical end-uses is always further limited by unavoidable losses associated with the available energy conversion routes. Every added conversion step in the process adds losses and reduces overall conversion efficiency.

A primary mechanism for converting solar energy on earth is the photoexcitation of electrons in terrestrial matter. With this electronic excitation as an initial step, the two basic routes for further energy conversion of the photoexcited electrons are *solar–thermal* and *solar-potential*. In the *solar–thermal routes*, the energized electrons thermalize to their surroundings, converting the energy to heat, which can be converted further, for example, using heat engines to produce work. Such routes are further restricted by lower Carnot limits based on the intermediate source temperatures driving the heat engines. In the alternative *solar-potential* routes, the elevated electrochemical potential of the energized electrons can directly drive further conversion processes, for example, producing electricity or chemical products. Thermal energy is not being converted to heat, so additional Carnot limits are not imposed.

Based on these photoexcitation models for energy exchange, solar water-splitting for hydrogen production can follow several different conversion routes, as shown in Fig. 7.4. The solar–thermal route shown as process (A) in the figure is a two-step process, with a photon-to-thermal energy conversion step followed by a thermal-to-chemical (TC) conversion step. The other two-step process shown as process (B) represents PV-electrolysis, where a photon-to-electric conversion step is followed by an electric-to-chemical conversion process. The three-step process (C) represents a concentrated-solar–thermal–electricity/electrolysis route, involving photon-to-heat, heat-to-electricity, and electricity-to-chemical conversion steps. The final pathway depicted as process (D), representing a single-step direct conversion from photon-to-chemical energy, is the PEC water-splitting process.

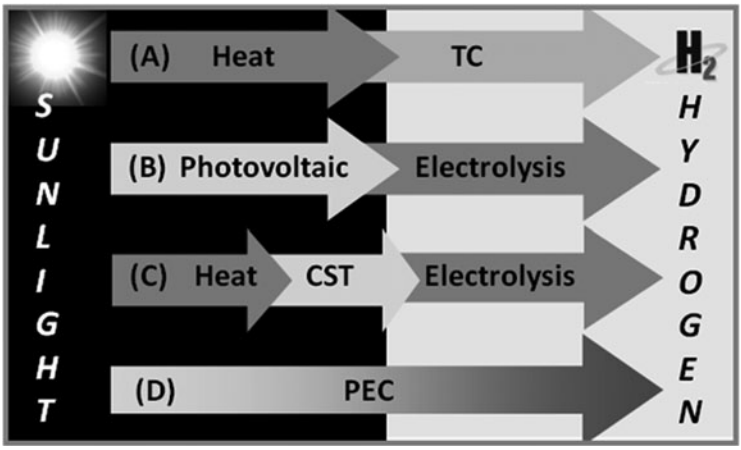

Fig. 7.4 Four viable single and multistep solar-to-hydrogen conversion pathways

Although a direct route in theory, practical implementation, for example, with multijunction semiconductor devices, will entail thermal losses which need to be minimized for high-efficiency conversion. Other STH pathways are also possible, including photobiological routes [31, 32] and the ultrahigh temperature thermolysis route [33], all with their own sets of challenges.

A number of different pathways can contribute to the renewable production of hydrogen for future "Green Economies," but economics will determine which ones will play the most important roles. In general, the most direct conversion processes, such as PEC water-splitting, could have some inherent economic advantages. In fact, PEC hydrogen production as a low-temperature single-stage process could be one of the front-running alternatives, contingent on development of sufficiently efficient, stable, and inexpensive material systems. Under the general umbrella of PEC solar hydrogen production, there are several possible plant strategies and configurations that could be practically feasible. These are described below.

7.2.4 Photoelectrochemical Hydrogen Plants

There are numerous hydrogen-production approaches utilizing solar energy for the PEC water splitting. With these different approaches, there are several possible commercial scale plant configurations [34, 35]. Ultimately, the practicality of any plant will be measured by the cost of the produced hydrogen. This will be determined by the efficiency, cost, and lifetime of the active PEC materials used, in addition to associated plant capital costs and operating expenses. As discussed in the following section, initial techno-economic analyses have been performed to compare and contrast economic advantages and disadvantages of different PEC plant concepts [35], but more comprehensive follow-on analyses will be needed,

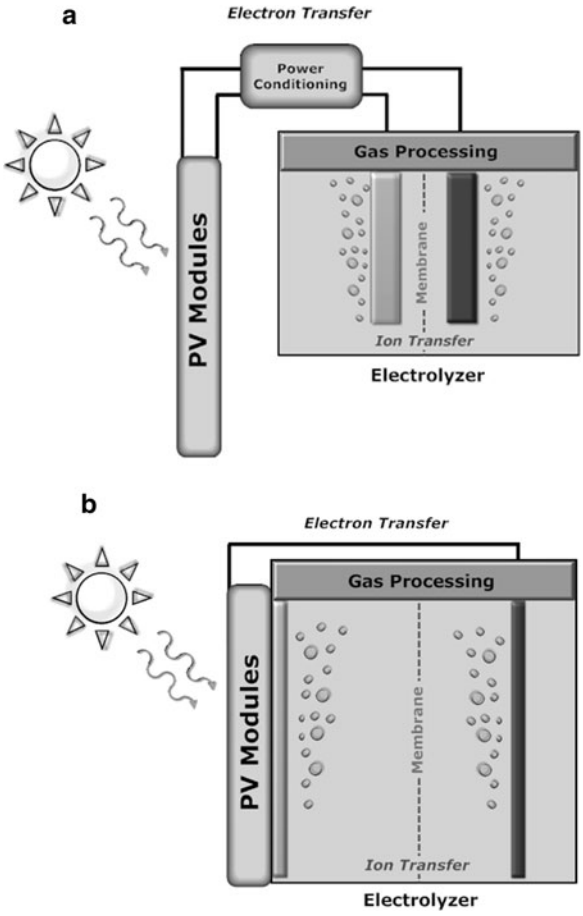

Fig. 7.5 (**a**) Interconnected PV–electrolyzer system with power conditioning unit; (**b**) area-matched integrated PV–electrolyzer system

especially as PEC conversion processes evolve and become more refined. Broadly speaking, PEC plant configurations fall into three categories: (1) combined PV-electrolysis systems; (2) photoelectrode-based systems; and (3) photocatalyst-based slurry systems. Many of the different single- and multijunction PEC materials and devices discussed in the following sections can be integrated into one or more of these plant types. Hydrogen production scales ranging from small-scale 1,500 kg/day for distributed production up to large-scale 50,000 kg/day central-plant production are being envisioned for all three categories. Some of the likely reactor schemes are illustrated in the following figures.

Figure 7.5a, for example, illustrates the most direct implementation of the "Combined PV-electrolysis" configuration. Commercially available photovoltaic (PV) panels are coupled with separate commercial electrolyzer units, such as alkaline or PEM electrolyzers; and appropriate power-conditioning equipment is utilized to load-match the processes. This is the clear path to near-term renewable solar hydrogen, but it is by no means inexpensive. Based on recent cost studies from the NREL, hydrogen production cost would exceed $10/kg for PV electricity cost at

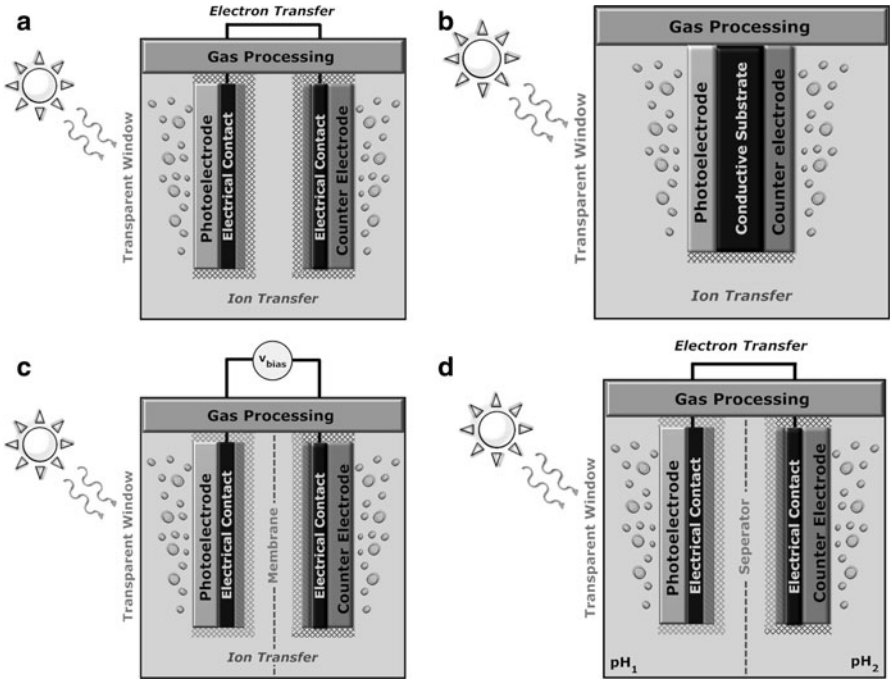

Fig. 7.6 (**a**) Two-electrode PEC system; (**b**) monolithically integrated single-electrode PEC system; (**c**) two-electrode PEC system with external voltage biasing; (**d**) two-electrode PEC system with chemical biasing

15–25¢/kW h [36, 37]. The need for power conditioning equipment contributes to this high cost. Additional factors include the electrolyzer capital costs as well as the losses from lateral collection and transmission of electricity.

A variation of the PV-electrolysis approach is the integrated PV-electrolyzer unit shown in Fig. 7.5b. In such systems, the solid-state PV panels and large area electrolysis components are designed to be better matched in terms of both operational voltage and current density. Power conditioning is eliminated and transmission losses would be reduced. Based on the direct coupling to the solar flux rage, the electrolysis process would run at low current densities, for example, below 50 mA/cm^2, compared with rates over 1,000 mA/cm^2 in commercial electrolyzers. This relaxes the need for precious metal catalysts in the electrolysis process, and therefore reduces capital cost. Added complexity and cost of the dual-function panels for large-scale deployment is a significant tradeoff.

Unlike the systems in the "PV-electrolysis" category, the photoactive components in the "photoelectrode based systems" configuration are immersed in solution, and typically include one or more PEC solid/liquid rectifying junctions.

Figure 7.6a shows a classic two-electrode configuration with a photoelectrode immersed in aqueous solution and electrically interconnected to a metallic counter electrode. Sunlight incident on the photoelectrode energizes the water-splitting

process, promoting hydrogen evolution at the "cathode" surface and oxygen evolution at the "anode" surface. The PEC process entails both electron exchange in the external wire and ion exchange in solution. To minimize electronic and ionic conductivity losses, the counter electrode is placed in close proximity to the photoelectrode surface. In some cases, the counter electrode is a small catalyst wire placed right in front of the photoelectrode. This, however, introduces some optical shading loss; and it also requires a front-surface gas-separation membrane, adding further loss.

Figure 7.6b illustrates a single-electrode variation of the photoelectrode system comprising anode and cathode surfaces at opposite faces of a single monolithically integrated device. In this configuration, electron transfer is readily achieved through the body of the electrode, but pathways for ionic transfer in the electrolyte need to be provided around the electrode body to minimize solution conductivity losses. Electron transmission loss is reduced, as is system part count. This offers potential cost reduction.

The photoelectrode schemes in Fig. 7.6a, b require photoactive electrode materials and devices capable of spontaneously splitting water with solar illumination. As discussed at length in the following sections, this will most likely require the use of multijunction structures to generate sufficient voltage to sustain the process. Alternative external-voltage and chemical biasing strategies are possible in photoelectrode-based systems as illustrated in Fig. 7.6c, d. External biasing is specifically useful for single-junction photoelectrodes incapable of efficient unassisted solar water splitting. The added costs associated with the supplemental electricity needed in Fig. 7.6c or chemical feedstocks needed to maintain the pH gradient in Fig. 7.6d generally makes these approaches unattractive from a practical perspective.

In the photoelectrode-based systems, active semiconductor layers or thin-films are coated on fixed electrode structures which are immersed in solution. In contrast, the "photocatalyst"-based reactors utilize photoactive semiconductor particles free-floating as slurry in a solution bed. Figure 7.7a represents a conceptual single-bed photocatalyst reactor, comprising concentrations of one or more functionalized photocatalyst particles suspended in solution. In the example shown in Fig. 7.7a, the semiconductor particle would need to be capable of internally generating enough photovoltage to split water. In addition, specific surface sites on the particle would need to be functionalized, for example, with catalyst nanoparticles, to promote hydrogen and oxygen evolution and facilitate charge separation. An interesting variation of the single-bed photocatalyst system is the "Z-scheme," which is somewhat analogous to the multijunction approach in the photoelectrode case. As described in more detail in later sections, the Z-scheme utilizes different photocatalysts for hydrogen and oxygen evolution, but the two particle types are mixed together in the same reactor bed with an ion mediator in solution to couple the reactions. Single-bed photocatalyst reactors are extremely simple, with perhaps the best potential for low cost at large scales. The obvious drawback is that potentially explosive mixtures of hydrogen and oxygen gas are generated in the same solution, necessitating safe and reliable gas separation mechanisms.

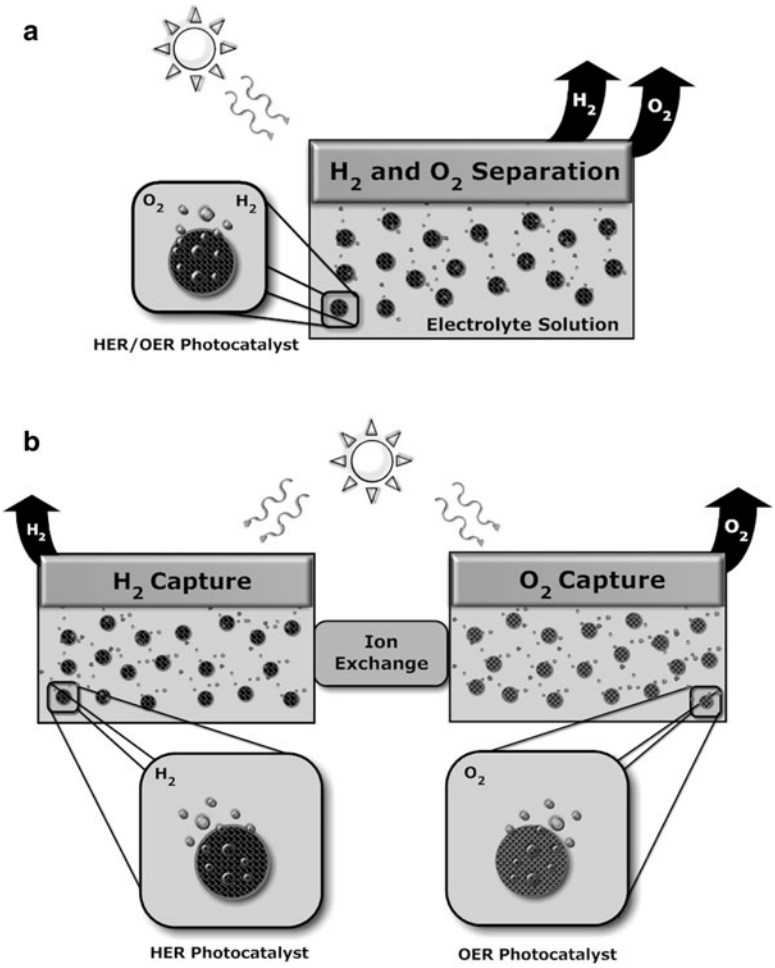

Fig. 7.7 (**a**) Single-bed photocatalyst particle suspension system, co-generating oxygen and hydrogen in the same reactor; (**b**) two-bed photocatalyst particle suspension system, with separated oxygen-evolution and hydrogen-evolution beds

Separation technologies, such as pressure swing absorption, are commercially available, but would add complexity and cost.

Figure 7.7b illustrates a two-bed photocatalyst reactor. Similar to the Z-scheme, two separate photocatalyst particles are used, one for hydrogen evolution and the other for oxygen evolution. In the two-bed case, however, the different particle types are suspended in separate reactors which are connected by an ionic bridge-way to allow for mediator coupling. In the two-bed reactors, the hydrogen and oxygen gases are generated separately and safely, eliminating the cost of separations equipment. The drawback is the reduced hydrogen production efficiency inherent in this configuration. The ion bridge introduces conductivity loss; but more importantly, a larger

solar collection area is necessary for water splitting when hydrogen and oxygen reactions are stacked side-by-side, reducing conversion efficiency and increasing overall cost.

7.2.5 Techno-economic Analyses

The US Department of Energy (DOE) recently commissioned *Directed Technologies Inc*. (DTI) of Arlington, Virginia, to conduct a techno-economic evaluation of conceptual PEC hydrogen production systems [35] incorporating performance and processing cost feedback from the broader materials R&D efforts at DOE. The objective was to provide a basis for evaluating the long-term feasibility of large-scale PEC production technologies in comparison with other renewable approaches. The DTI study, which was completed in 2009, comparatively evaluated two photocatalyst particle bed configurations (compatible with the reactor configurations illustrated in Fig. 7.7) as well as two photoelectrode-based systems (compatible with the reactor configurations illustrated in Fig. 7.6). The four conceptual systems in the study were designated "Type-1" through "Type-4" as follows:

- *Type-1: Single-Bed Photocatalyst System*: A single electrolyte-filled reactor bed containing a colloidal suspension of PEC photocatalyst particles which produce a mixture of H_2 and O_2 product gases.
- *Type-2: Dual-Bed Photocatalyst System*: Two electrolyte-filled reactor beds containing colloidal suspensions of PEC photocatalyst particles, with one bed carrying out the oxygen evolution half-reaction, the other bed carrying out the hydrogen evolution half-reaction, and including a mechanism for circulating the ions between beds.
- *Type-3: Photoelectrode System*: A fixed array of planar PEC photoelectrodes immersed in an electrolyte reservoir, tilted toward the sun at local latitude angle, producing hydrogen at atmospheric pressure.
- *Type-4: Photoelectrode System with Moderate Concentration*: A PEC solar concentrator system, using reflectors to focus the solar flux at a 10:1 intensity ratio onto planar PEC photoelectrodes immersed in an electrolyte reservoir and pressurized to 300 psi.

In the DTI analyses, each of the modeled system types included a PEC reactor generating H_2 and O_2: photocatalyst-based on Types 1 and 2, and photoelectrode-based on Types 3 and 4. Each also included a gas processing system for compressing and purifying the output gas stream, in addition to ancillary balance of plant equipment. For each system type, the total cost of hydrogen production was projected for a 10-metric ton per day plant assuming technology-readiness of the PEC reactor. The baseline for readiness included targeted values of 10% for STH conversion efficiency and 5 years for PEC cell lifetimes. Sensitivity analyses around the baseline assumptions were performed to assess the effects on production

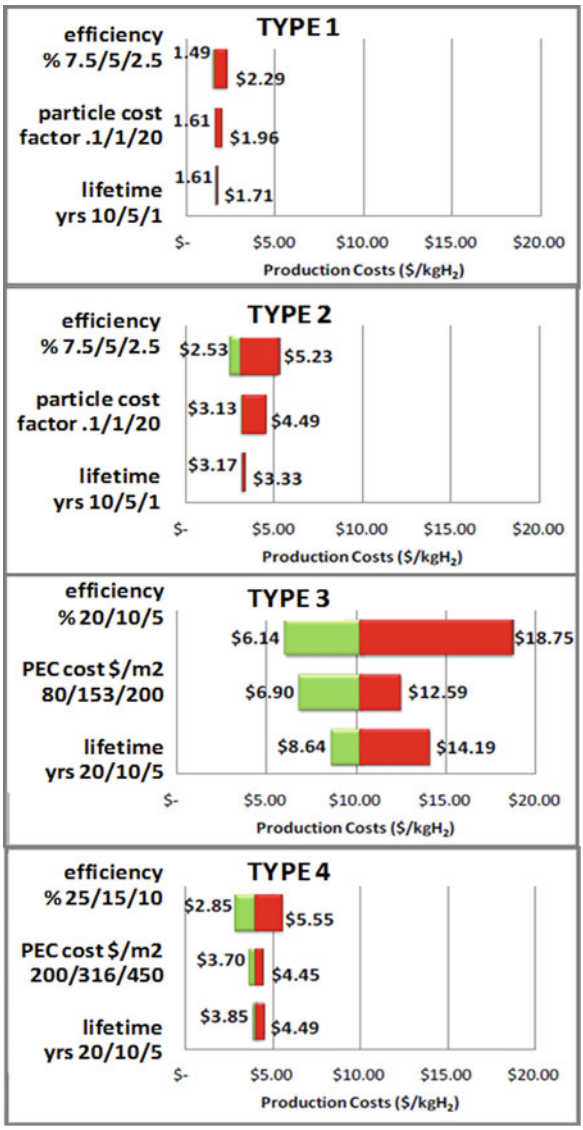

Fig. 7.8 Hydrogen cost sensitivity analyses for the four reactor types evaluated in the DTI techno-economics report on *Photoelectrochemical Hydrogen Production*. Projected hydrogen costs as a function of efficiency, lifetime, and materials cost are shown

costs of variations in the PEC performance and cost parameters. A summary of the sensitivity analyses for the four system types is shown in Fig. 7.8.

As concluded in the DTI report, the hydrogen production costs are lowest for the Type 1 and Type 2 photocatalyst systems, ranging from \$1.50 to \$5.25/kg H_2. These are encouraging results, consistent with the US DOE cost targets of \$2–4/kg H_2 [38] for future central hydrogen production pathways. The report recognized, though, that significant research and development work is still needed to demonstrate particle-based PEC reactors operating at the baseline performance levels

assumed in the study. In contrast, the Type 3 photoelectrode system is currently the most mature of the concepts, with numerous prototypes demonstrated to date on the laboratory scale. The report concluded, however, that hydrogen production costs were the highest using this route, ranging from \$6.14 to 18.75/kg H_2. The high costs in this case were dominated by substantial material and capital costs, similar to those plaguing the PV industry. The Type 4 photoelectrode system is a modification of Type 3 system with the addition of modest solar concentration (up to 10×) and moderate internal hydrogen compression (to 300 psi). Interestingly, these added features resulted in substantial cost reductions, specifically due to the reduction in PEC-electrode area, reduced amount of PEC materials needed, and fewer postprocessing compression stages. The resulting hydrogen production costs were reduced to \$2.85–5.55/kg H_2, falling within the DOE targeted range.

Although preliminary, this study has shown that hydrogen production by PEC systems can be economically viable in both photocatalyst and photoelectrode configurations. However, key research challenge remains for attaining PEC material systems compatible with the baseline levels of 10% STH conversion efficiency and 5-year lifetime. As discussed in the following sections, multijunction approaches are likely to be critical for near-term realization of such performance levels. As research and development of PEC materials and devices progresses, more techno-economic analyses will be needed to further evaluate the tradeoffs between different large-scale PEC reactor approaches. Two of the most promising avenues appear to be photoelectrode systems using low-cost thin-film materials [39] and large-scale slurry bed reactors utilizing low-cost functionalized semiconductor particles [40]. The path forward for practical PEC solar hydrogen production needs to navigate all the economic as well as the scientific obstacles that remain.

7.3 Photoelectrochemical Water Splitting

In general, standard chemical processes involve interactions between chemical and ionic species. Electrochemical processes also involve interfacial interactions between ionic conductors, such as electrolytes, and solid-state electronic conductors, such as semiconductors. Involving even more complexity, PEC processes are exposed to light, so that optical photons can also interact with the electrochemical reactions. In semiconductor photoelectrochemistry, energetic photons of light typically create electron–hole pairs within the semiconductor that can participate in redox reactions at the semiconductor/electrolyte interfaces. The complicated set of fundamental electrochemical and solid-state optoelectronic principles that govern the behavior of such systems are well-documented in the literature [41–46]. Within the realm of photoelectrochemistry, the PEC water-splitting process itself presents a unique set of energetic and kinetic challenges [47–50]. Some useful simplifications to the problem, presented in the following sections, can provide a broad overview of PEC water-splitting, and help to highlight the loss mechanisms and conversion efficiency limitations inherent in PEC hydrogen production.

7.3.1 PEC Water-Splitting Reactions

Any light-driven water splitting process can be expressed as a generalized chemical reaction representing the addition of photonic energy to liquid water to split the H_2O molecule, evolving gaseous hydrogen and oxygen:

$$H_2O + 2\gamma \rightarrow H_2(g) + 1/2O_2(g) \quad \text{Net water-splitting reaction} \tag{7.1a}$$

$$\Delta G^0 = +237.18 \text{ kJ/mol} \quad \text{Standard Gibbs free energy.} \tag{7.1b}$$

Here, γ is the photon energy and ΔG° is the standard Gibbs free energy. As indicated in (7.1), energetic photons, such as those in sunlight, can supply the energy to drive the uphill reaction converting the feedstock H_2O into hydrogen and oxygen gases. Specifically, the standard Gibbs free energy change of +237.18 kJ/mol is a quantification of the thermodynamic minimum energy needed for splitting water into the constituent gases at standard conditions of 25°C and 1 bar.

PEC implementations of light-driven water splitting utilize one or more photoactive semiconductor electrodes to convert the photon energy. In a PEC system, absorbed photons induce electron–hole pairs in the semiconductor bulk which can be separated and extracted to promote two "half reactions" in solution. Specifically, photogenerated electrons drive the hydrogen evolution half-reaction (HER) at the cathode interface, while photogenerated holes drive the oxygen evolution half-reaction (OER) at the anode interface. Both half reactions must be sustained simultaneously, coupled by their exchange of electrons in the solid state, and ions in solution. In real systems, multiple reaction pathways and reaction steps are possible at both anode and cathode, and physical conditions shape if and how the process will proceed. As one example, the half-reactions for water splitting can be written explicitly in terms of the H^+ ionic exchange between anode and cathode:

$$2\gamma \rightarrow 2e^- + 2h^+ \quad \text{Photon-induced electron-hole pair generation} \tag{7.2a}$$

$$H_2O + 2h^+ \rightarrow 2H^+ + 1/2O_2(g) \quad \text{OER: anodic water-oxidation half-reaction} \tag{7.2b}$$

$$2H^+ + 2e^- \rightarrow 2H_2(g) \quad \text{HER: cathodic } H^+\text{reduction half-reaction} \tag{7.2c}$$

$$H_2O + 2\gamma \rightarrow H_2(g) + 1/2O_2(g) \quad \text{Net water-splitting reaction} \tag{7.2d}$$

$$\Delta G^0 = +237.18 \text{ kJ/mol} \quad \text{Standard Gibbs free energy} \tag{7.2e}$$

$$\Delta V^0_{rev} = \Delta G^0/nF = 1.23 \text{ V} \quad \text{Standard reversible potential} \tag{7.2f}$$

$$V_{op} = \Delta V^0_{rev} + \eta_a + \eta_c + \eta_\Omega + \eta_{sys} \quad \text{Operating voltage with overpotential loss.} \tag{7.2g}$$

Here, e^- is an electron, h^+ is a hole, F is Faraday's constant, and n (=2) is the number of electrons exchanged. V_{op} is the operational voltage, η_a, η_c, η_Ω, and η_{sys} are overpotentials associated with anode, cathode, ionic-conductivity, and system losses, respectively.

Alternatively, the half-reaction set can also be written in terms of OH^- ionic exchange:

$$2\gamma \rightarrow 2e^- + 2h^+ \quad \text{Photon-induced electron-hole pair generation} \tag{7.3a}$$

$$2OH^- + 2h^+ \rightarrow H_2O + 1/2O_2(g) \quad \text{OER: half-reaction} \tag{7.3b}$$

$$2H_2O + 2e^- \rightarrow 2OH^- + H_2(g) \quad \text{HER: half-reaction} \tag{7.3c}$$

$$H_2O + 2\gamma \rightarrow H_2(g) + 1/2O_2(g) \quad \text{Net PEC water-splitting}. \tag{7.3d}$$

The corresponding expressions for the Gibbs free energy, the standard reversible potential and the operating voltage are equivalent to those given by (7.2e–g).

The reaction pathways depend on the nature of the electrodes, the electrolyte, and the light-induced energy levels. For example, the half-reaction formulations expressed in terms of H^+ tend to dominate in acidic electrolyte solutions, while the OH^- formulations can dominate in basic solutions, specifically due to the predominance of one ionic species over the other under the different conditions [51]. In either case, it is important to emphasize that each of the half-reactions described in (7.2) and (7.3) is simplifications of more complex multistep electrochemical reaction pathways, and that competing or parasitic reactions are also possible [52, 53]. Without parasitic reactions and losses, the Gibbs free energy of photo-driven water splitting is +237.18 kJ/mol, and the standard reversible potential of PEC water splitting is 1.23 V, as indicated in (7.2) and (7.3). This is independent of the dominant pathways involved in achieving the net reaction. All practical systems will involve losses, such as those represented in the various overpotential terms in the equations; and these losses can be significantly different for different reaction pathways. Including overpotential losses, the energy/voltage needed to split water will inevitably exceed 1.23 V.

7.3.2 PEC Water Splitting Losses

Losses incurred during PEC water splitting include the overpotential losses at the anode and cathode interfaces, the ionic conductivity overpotential loss associated with ion transport in the electrolyte, as well as other solid state and balance of system losses. The anode and cathode overpotential losses include the effects of activation energy, kinetics, and mass-transport of the multistage half reactions. These can be substantial, commonly several tenths of volts, with more severe loss

for oxygen evolution, which is the more complex and less facile reaction [54]. In addition to the electrode overpotential losses, the electrochemical losses due to ionic conductivity in the solution can also be severe, depending on electrode geometry and spacing, in addition to solution properties. The splitting of *pure water*, for example, is particularly difficult, since the ionic conductivity, typically less than 0.05 S/m range is prohibitively low. Weak acid or alkaline solutions with conductivities exceeding 10 S/m are typically used to compensate, although this creates a more corrosive environment for the electrodes.

On top of the losses at the interfaces and in solution, there are also significant losses in the solid state of any PEC system. While the ions in solution are migrating through the aqueous media and reacting at the interfaces, the solid-state electrons–holes need to be exchanged between the anode and cathode through a conductive pathway (such as an interconnecting wire in two electrode schemes and the conducting substrate in monolithic single electrode configurations), and therefore some ohmic loss is inevitable. Additionally, there can be severe losses in the bulk semiconductor and solid-state interfaces of the electrodes. These include optical absorption losses, electron–hole pair recombination losses, and interface recombination losses, among others, which also degrade system performance.

The PEC water splitting process is a delicate balancing act, where photon-energized electron–hole pairs under the right conditions can simultaneously drive the electrochemical half-reactions. In steady state, the anodic and cathodic half-reactions need to be sustained at the same reaction rate, or a charge build-up will occur, impeding and eventually stopping the entire process. A similar situation exists with the charge carriers in the solid state. The anodic half-reaction generates two electrons (i.e., "consumes" two holes), while the cathode half-reaction consumes two electrons. These electrons must be shuttled from anode to the cathode via electrical current and steady state cannot be maintained if anode and cathode reaction rates are not the same.

As a result of all the electrochemical, solid-state losses and any balance of system losses occurring at steady state, water splitting cannot occur at the bulk reversible potential of 1.23 V. The operating voltage for water-splitting must exceed this value to compensate for all the losses. In practice, water electrolysis systems typically require operating voltages of 1.6–1.9 V, depending on gas production rates [55, 56]. In other words, to drive the water-splitting process including all solution and electrode losses, the absorbed photons must induce sufficient electrochemical potential to the electron–hole pairs to generate photopotentials in excess of approximately 1.6 eV. The photoelectrolysis *balancing act* can be set into motion *ONLY* if this photopotential requirement is met. As discussed in the following sections, it is the photopotential requirement that may necessitate the use of multijunction approaches for efficient PEC water splitting. If and only if the conditions are right to sustain the water splitting process, the hydrogen evolution will then be proportional to electron consumption rate at the cathode, which represents a *photocurrent*. This is critical to the understanding of STH conversion efficiency.

7.3.3 PEC Solar-to-Hydrogen Conversion Efficiency

During steady-state operations, the solid-state shuttling of charges between anode and cathode represents a photon-induced current, or photocurrent. This photocurrent is integrally tied to the hydrogen-producing performance of the PEC system. Specifically, the PEC half reactions from the previous section illustrated that two electrons are consumed in the evolution of one H_2 molecule. This results in a hydrogen production rate that is half the rate of electron flow, in other words, half the photocurrent:

$$R_{H_2} = \frac{I_{ph}}{2e} = \frac{\left(J_{ph} \times A\right)}{2e}, \tag{7.4}$$

where R_{H_2} is the hydrogen production rate (s^{-1}), I_{ph} is the photocurrent (A), e is the charge of an electron (C), A is the area of the illuminated photoelectrode (m^2), and J_{ph} is photocurrent density (A/m^2).

The chemical STH conversion efficiency of a solar-based hydrogen production system is defined as the ratio of the useable chemical energy in the generated hydrogen gas to the total solar energy delivered to the system [57–61]. For steady-state operations, this is equivalent to the ratio of the *power output* to *the power input* of the system. This power ratio can be expressed as:

$$\frac{P_{out}}{P_{in}} = \frac{(\text{hydrogen production rate}) \times (\text{hydrogen energy density})}{\text{solar flux integrated over illuminated area}}. \tag{7.5}$$

Using the hydrogen production rate from (7.4) and the Gibbs energy as the useful energy density of the hydrogen, the STH efficiency for a PEC system can be written as:

$$\text{STH}(\%) = \frac{\frac{\Delta G}{N_A} \times R_{H_2}}{P_{solar} \times A} = \frac{\frac{\Delta G}{N_A}\left(\frac{J_{ph} \times A}{2e}\right)}{P_{solar} \times A} = \frac{\frac{\Delta G}{2eN_A}}{P_{solar}} \times J_{ph}, \tag{7.6}$$

where N_A is Avogadro's number and P_{solar} is the solar flux of energy in W/m^2. The first ratio in (7.6) is generic for any STH production system, while the second term is derived specifically for PEC hydrogen processes using the production rate from (7.4).

The solar flux of radiant energy is comprised of a broad spectrum of energetic photons, which are quantized particles of light, each with discrete energy content. Figure 7.9a shows the standard atmosphere-filtered global solar spectrum (AM1.5G) indicating the range of photon energies and the distribution of energy transmitted by these photons [62]. This AM1.5G spectrum is also frequently presented as a function of photon wavelength, as shown in Fig. 7.9b.

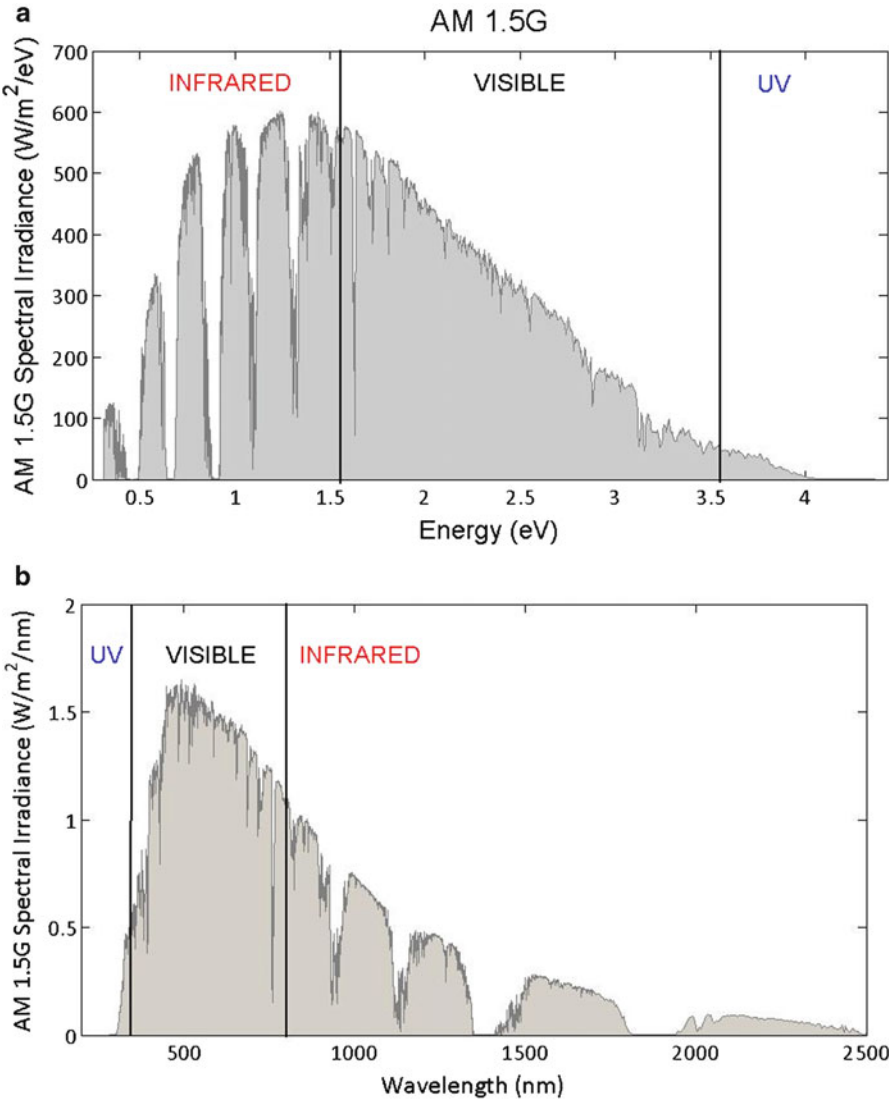

Fig. 7.9 AM1.5 global solar irradiance spectrum: (**a**) as a function of photon energy and (**b**) as a function of photon wavelength, indicating the ultra-violet, visible, and infra-red regions of sunlight

Integrating the AM1.5G solar flux yields a total power density of ~1,000 W/m^2 for sunlight. Using this value for P_{solar} in (7.6), the STH conversion efficiency can be related directly to the photocurrent density of a PEC system:

$$\text{STH}_{\text{AM1.5}}\ (\%) \approx \underbrace{0.123 \times J_{\text{ph}}}_{\text{for } J \text{ in}(\text{A/m}^2)} = \underbrace{1.23 \times J_{\text{ph}}}_{\text{for } J \text{ in}(\text{mA/m}^2)} . \tag{7.7}$$

Equation (7.7) explicitly states the linear relationship between conversion efficiency and photocurrent density calculated under AM1.5G solar illumination. The use of the Gibbs free energy in these equations reflects chemical energy in the hydrogen that can be retrieved using an ideal fuel cell. This in effect, calculates the lower heating value (LHV), which is standard in practical comparisons between different fuels [63].

It is clear from (7.7) that the PEC photocurrent density is the key determining factor for STH efficiency. This is in contrast to solid-state photovoltaic cells, which need to be operated at the *maximum power point* (i.e., maximum product of photocurrent and photovoltage) for the best solar-to-electric conversion efficiency [64]. It is a subtle but important distinction that PEC cells should be operated at maximum photocurrent for best hydrogen-production performance. It is the bandgap-limited *saturated photocurrent density* of a semiconductor that ultimately constrains the hydrogen production rate. For peak STH efficiency, sufficient useable photopotential must be generated in the device to drive the photocurrent as close as possible to the saturation limit. With all the built-in losses in the solid state, in solution, at the interfaces, and in the balance of system, this can be a challenge. In fact, due to limits of useable photopotential generation in a single junction, it may be necessary to resort to multijunction schemes to drive the PEC system into the maximum photocurrent region. There are inherent trade-offs and limitations as well as benefits to this approach. These are explored in detail in the following sections.

7.4 Single Junction PEC Semiconductor Devices

In a semiconductor-based PEC system, photons are absorbed in the semiconductor and the photogenerated charge carriers are separated, and then extracted by the interfacial HER and OER reactions. In photoelectrode-based systems, the charge separation is largely due to the rectifying nature of the semiconductor/electrolyte junction. The charge separation details are somewhat different in the photocatalyst systems [65], but the basic absorption and extraction mechanisms at the solid/liquid interface are the same. In either case, hydrogen production performance is strongly influenced by both semiconductor material properties and interfacial characteristics. An examination of junction formation and operation in the case of photoelectrode configurations reveals much about the key performance parameters and conversion efficiency limitations.

7.4.1 Photoelectrode Junction Formation

In PEC photoelectrode systems, the semiconductor/electrolyte interface can form a *rectifying* junction, similar to the solid-state pn junctions or Schottky diode junctions used in solar cells. Such rectifying junctions exhibit built-in electric fields

capable of separating photogenerated charge carriers (i.e., electron–hole pairs) created by absorption of photons in the semiconductor bulk. In PV cells, this charge separation mechanism drives photocurrents to produce electricity, while in the PEC case, the charge separation can drive the HER and OER half-reactions for water splitting. In both cases, illumination creates extra photoexcited electron–hole pairs which need to be separated and extracted before they recombine in order to be effective in the energy conversion process. Extraction of the photogenerated charge carriers with elevated electrochemical potentials in effect converts the solar energy to electricity or hydrogen in PV or PEC systems, respectively. Excellent sources of information are available detailing semiconductor material properties, solid-state junctions and solar cells, and treating the fundamentals of rectifying junction formation and behavior [26, 50, 66–70].

Formation of a rectifying PEC junction at a semiconductor/electrolyte interface follows similar principles, but key concepts from both solid-state physics and electrochemistry need to be combined for a complete description of the process. For reference, there is a wealth of literature on fundamental electrochemical principles [41–46, 50], which are useful, especially in conjunction with the previous citations covering semiconductor physics. Of particular interest to PEC studies are the models developed by Gerischer, which establish important connections between the in-solution electrochemical potentials of electrons and solid-state Fermi levels [47–49]. Using the Gerischer models, descriptions of semiconductor/electrolyte junctions follow closely the solid-state junction analogies. Photoanodes using n-type semiconductors form PEC junctions similar to a Schottky barrier or an np^+ junction, and internal electric fields are set up to drive photogenerated holes toward the electrolyte interface promoting oxygen evolution. In contrast, p-type photocathode junction formation is analogous to a solid-state pn^+ device, and the internal fields promote the injection of photogenerated electrons at the interface to drive the HER [50]. The field directions for both n-type and p-type junctions are shown explicitly in the following illustrations of junction formation.

Specific steps in semiconductor/electrolyte junction formation are illustrated in Fig. 7.10 for both the photoanode (7.10a) and photocathode (7.10b) cases. In Fig. 7.10a (i), the n-type semiconductor and electrolyte are shown in thermal equilibrium prior to contact for the photoanode case. At equilibrium, the Fermi level in the semiconductor (F_n) is close to the conduction band (CB), and the Fermi level in solution (F_s) falls between the redox (reduction/oxidation) levels for hydrogen reduction (H^+/H_2) and water oxidation (H_2O/O_2). After contact, the electrode and electrolyte Fermi levels align to reach thermal equilibrium, as shown in Fig. 7.10a (ii). Since the initial electrode Fermi level is higher than the electrolyte Fermi level, free electrons in the n-type semiconductor will migrate to the solid–liquid interface exposing positively charge fixed donor sites. The electrons form a surface charge layer at the interface which induces a thin Helmholtz double layer in the electrolyte. A *depletion-region*, also known as a *space-charge region* (SCR), forms where free charge carrier diffusion is counter-balanced by the built-in electric field generated by the fixed charges flanking the junction. The charge distributions including the fixed space charges in the solid-state electrode and the Helmholtz layer charges in solution are shown in Fig. 7.10a (iii). Typically, Helmholtz layers are on the

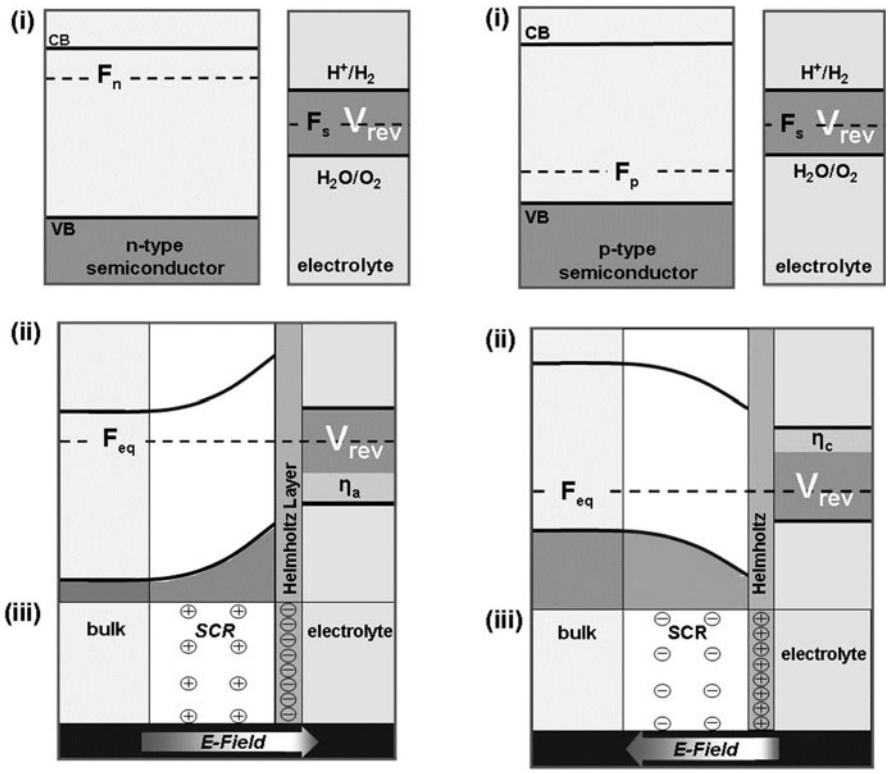

Fig. 7.10 Semiconductor/electrolyte junction formation for (**a**) n-type semiconductor and (**b**) p-type semiconductor junction. Subheadings (**i**), (**ii**), and (**iii**) represent the energy diagrams before contact, the energy diagrams after contact, and the charge distributions, respectively

order of a few nanometers, compared with several micrometers for the semiconductor space-charge region.

For the p-type photocathode case, the equilibrium charge distribution process is the same, but as shown in Fig. 7.10b the charges and band bending are reversed. As illustrated in Fig. 7.10b (i) and (ii), the initial migration of holes toward the interface during contact equilibration creates a space charge region of fixed negative acceptor charges, reversing the direction of the built in electric field compared with the photoanode cases. In both cases, the thermal equilibrium is disturbed upon exposure to light, and illuminated operations need to be described in terms of "quasi-equilibrium" statistics, which generally remain valid for AM1.5G insolation as well as moderate levels of concentrated sunlight [66, 67, 70].

7.4.2 Illuminated Response

Under illumination, the electron–hole pairs generated by photon absorption in the vicinity of the space-charge regions can be separated by the built-in electric

fields. Some of the photocharges will be successfully extracted in the water splitting process, while the remainder will recombine, losing energy as radiation or heat. In the photoanode case, the photogenerated holes will be driven by the built-in field toward the electrolyte interface, where, with the appropriate energetics and kinetics, they can drive the OER oxidation reaction. At the same time, photoexcited electrons are driven toward the electrode's back contact, where they can be extracted to solution at counter-electrode surfaces appropriately conditioned to promote the HER. For photocathodes, the charge separation supplies photogenerated electrons to the hydrogen evolution process at the electrolyte interface, and drives photogenerated holes to an OER counter electrode surface. Under these operating conditions, the initial thermal equilibrium has been disturbed by the energy influx of the light, and the band descriptions with Fermi levels are no longer valid. Under conditions of quasi-equilibrium, a useful alternative description can be developed in terms of "quasi-Fermi" levels.

Figure 7.11 illustrates PEC junction response to solar illumination for both photoanodes (Fig. 7.11a) and photocathodes (Fig. 7.11b) using the quasi-Fermi level descriptions. For both configurations in Fig. 7.11, the photoelectrode is immersed in solution, and the back contact is connected by external wiring to a counter electrode also in solution. In addition, the η_a and η_c overpotentials for the OER and the HER in solution have been added to the reversible potential of the redox system to stress the minimum voltage requirement to sustain water splitting.

With the absorption of sunlight in the semiconductor bulk, the original Fermi levels split into separate quasi-Fermi levels for electrons (F_e) and holes (F_h) [47, 66, 67, 70] resulting from the excess concentration of photogenerated electron–hole pairs over the equilibrium populations. For the photoanode case in Fig. 7.11a, the excess hole population significantly alters the minority carrier distribution with respect to the equilibrium populations, while the excess electrons barely affect the majority carrier numbers. As a result, the hole quasi-Fermi level shifts substantially in contrast to insignificant change in the electron quasi-Fermi level. Conversely, in the photocathode case in Fig. 7.11b, there is a significant shift in the electron quasi-Fermi level, but little hole quasi-Fermi level shift. In both cases, near the back contact away from the effects of illumination, the two quasi-Fermi levels converge back to a bulk equilibrium Fermi level.

The back contact potential is tied to the counter electrode potential, which under operating conditions is coupled to the back half reaction. As an important result, the quasi-Fermi separation in the semiconductor determines the *useable* energy for driving the front half reaction. For the illuminated photoanode device shown in Fig. 7.11a, the electron potential at the counter electrode is sufficiently high to drive the hydrogen-reduction half-reaction, including the η_c loss. Simultaneously, the quasi-Fermi hole energy at the solution interface is sufficiently *low* to drive water-oxidation, including the η_a loss. This configuration, in consequence, is capable of sustaining the net PEC water-splitting process, driven by *useable* energy in the quasi-Fermi split.

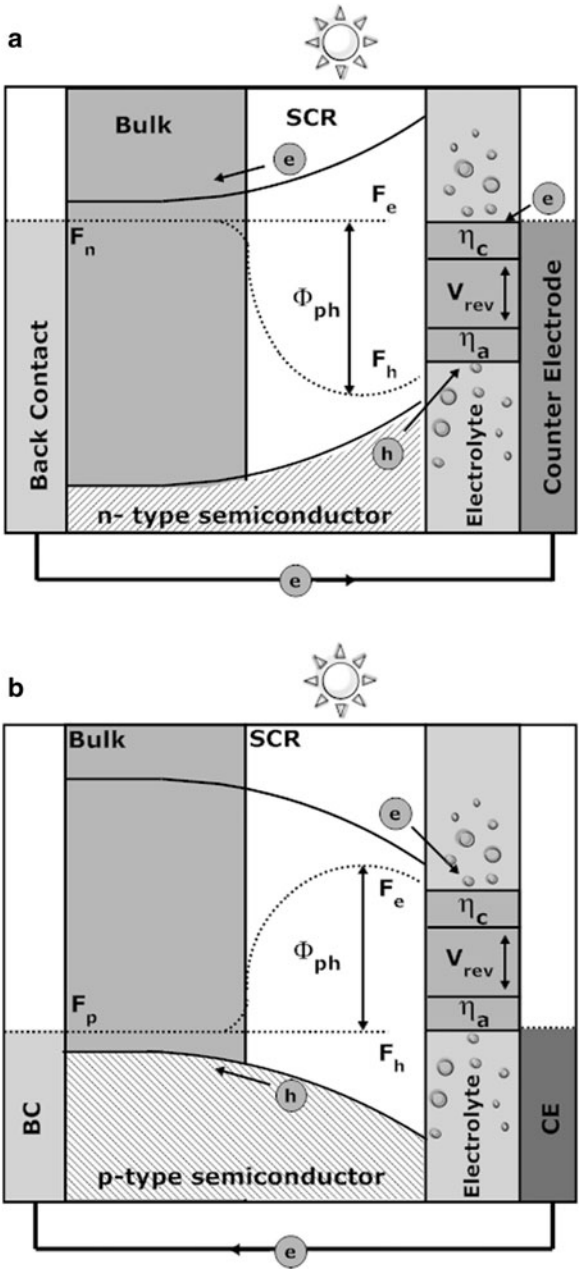

Fig. 7.11 Operational illuminated PEC junctions (**a**) n-type junction with correct hole energy alignment for oxygen evolution and electron energy alignment for hydrogen production, (**b**) p-type junction with correct electron energy alignment for hydrogen production and electron energy alignment for hydrogen evolution

7.4.3 Useable Photopotential

The concept of the quasi-Fermi level split is extremely important to how much *useable* photopotential a semiconductor device can generate, specifically in relation

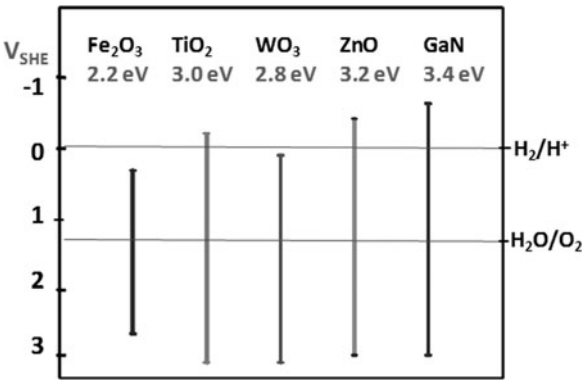

Fig. 7.12 Bandgap position of several common PEC semiconductors relative to the water-splitting redox potentials measured vs. the standard hydrogen electrode (SHE)

to the bandgap energy. In crystalline silicon photovoltaic cells, for example, the bandgap energy is 1.1 eV, while single-junction open-circuit voltages typically range between 0.6 and 0.7 V [26]. Thermodynamically, semiconductor band diagram representations reflect the *internal energy* of electrons and holes, not the *useable energy*. Electricity can be extracted from a PV cell only at potentials below the open-circuit voltage, which is typically 50–70% of the semiconductor bandgap energy. The output voltage limit can be increased using higher bandgap cells, but as a tradeoff, fewer solar-spectrum photons would be absorbed, limiting the saturated photocurrent.

The concept of useable potential is even more important in the case of PEC water-splitting devices. The useable potential of a PEC device must be sufficiently high to drive both half reactions in addition to the overpotential losses. This can typically require over 1.6–1.9 V. To achieve this in a single junction device, semiconductor bandgaps over 3.0 eV are typically necessary, which severely restricts optical absorption, saturated photocurrent, and therefore, STH conversion efficiency.

The bandgap position relative to the redox potentials of the electrolyte must also be considered. It is often reported that semiconductors with bandgaps "straddling" the redox potentials will be able to photosplit water in single junction configurations. While this is a "necessary" condition, it is by no means a "sufficient" condition. The band positions of semiconductor interfaces in aqueous solutions have been reported [5]. Figure 7.12, for example, shows the band edge positions with respect to the redox levels for hydrogen reduction and water oxidation for several commonly studied PEC semiconductor materials. Of these materials, titanium dioxide, zinc oxide, and gallium nitride all have bandgaps greater than 3 eV, and band edges straddling the redox levels. None of these, however, have demonstrated spontaneous PEC water splitting. This further drives home the point that the real energetics and useable photopotential under illumination are dictated by the quasi-Fermi levels, and not by the band edges. In addition, it is important to stress that all the overpotential losses directly subtract form useable potential. As a result, there are many situations where a bandgap straddling the redox potentials will fail to split water.

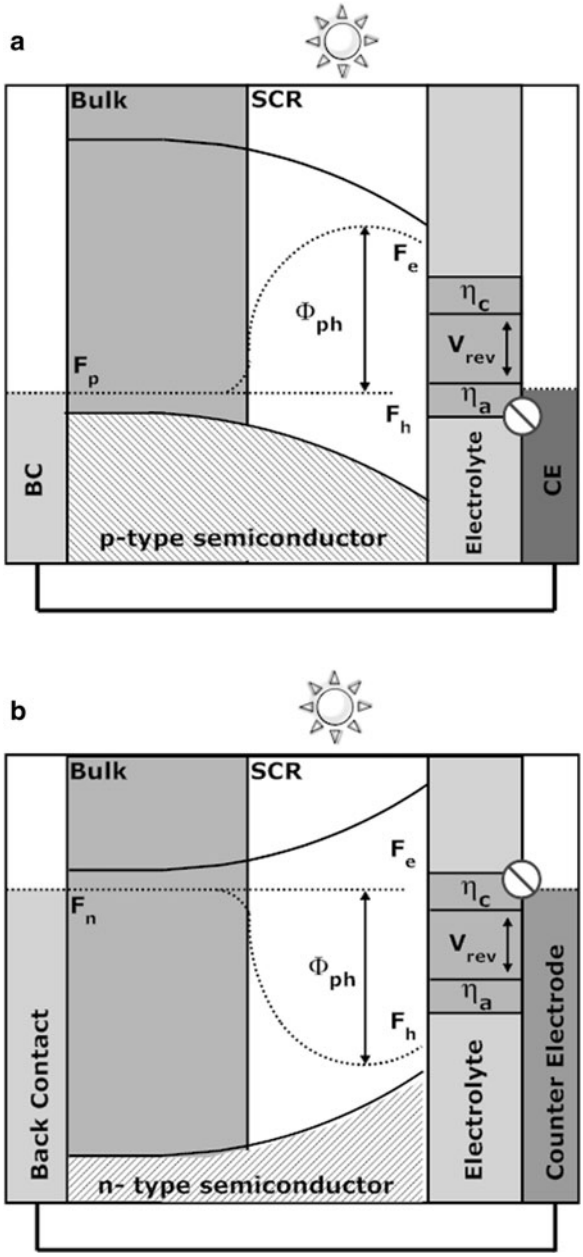

Fig. 7.13 Nonoperational illuminated PEC junctions (**a**) n-type junction with correct hole energy alignment for oxygen evolution but improper electron energy alignment for hydrogen production, (**b**) p-type junction with correct electron energy alignment for hydrogen production but improper electron energy alignment for hydrogen evolution

To illustrate this further, two additional hypothetical devices are illustrated in Fig. 7.13a, b representing photoanode and photocathode junctions, respectively, that are incapable of solar water splitting. In both cases, the conduction and valence band-edges clearly straddle the redox levels, even including the overpotential

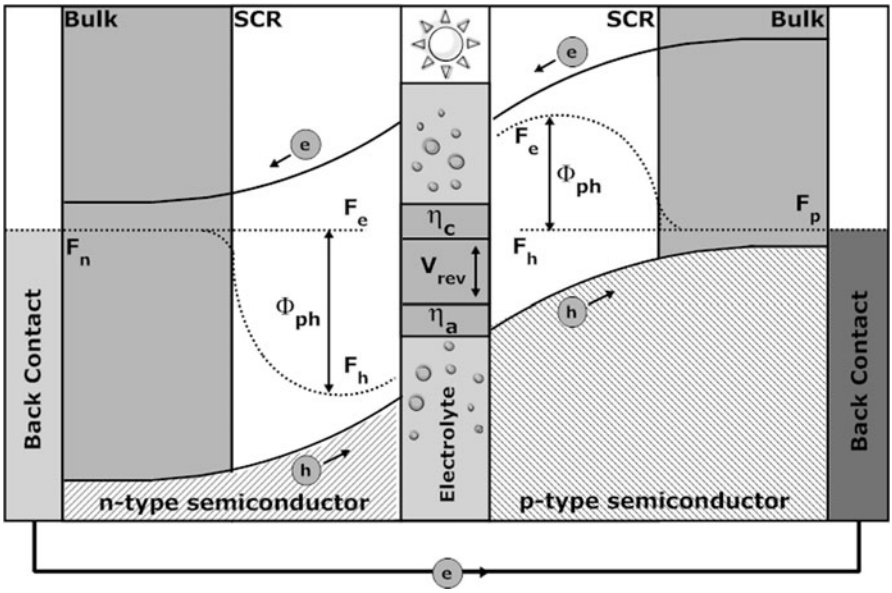

Fig. 7.14 Functional PEC–PEC tandem arrangement combining the nonoperational n-type and p-type electrodes from Fig. 7.13. There is Fermi level alignment at the interconnected back contacts, and the combined photopotentials developed in the two illuminated electrodes is sufficient to split water

losses. In Fig. 7.13a, however, the hole quasi-Fermi level at the PEC interface is too high, while in Fig. 7.13b, the electron potential in the counter electrode is too low and thus in either case PEC water-splitting is not sustainable.

Interestingly, these "dysfunctional" photoelectrodes could, in theory, be combined in tandem to achieve sufficient useable potential for water splitting. This is illustrated in the combined band-diagram representation seen in Fig. 7.14, where the two electrodes have been interconnected to each other, instead of to counter electrodes. This utilization of multiple junctions to enhance useable photopotential is a powerful tool for PEC water-splitting. As discussed in the following sections, multijunction stacking can offer important benefits, but can also introduce new system losses that limit overall STH conversion efficiency. In all single- and multijunction configurations, loss minimization in the device and system designs becomes critical to hydrogen production performance and efficiency.

7.4.4 Loss Minimization

There are numerous losses in PEC devices and systems that can limit STH conversion efficiency, and which need to be minimized. These include losses in solution,

at interfaces, and in the semiconductor bulk. The optoelectronic losses in the semiconductor photoelectrode, for example, need to be as low as possible. In single-junction absorbers, photons with energies below the semiconductor bandgap cannot be absorbed or converted. Photons with energies exceeding the bandgap are absorbed, but at rates dependent on the allowed transitions in the semiconductor. Direct bandgap materials, for example, absorb more efficiently than indirect bandgap materials. In all semiconductors, photogenerated electron–hole pairs rapidly thermalize to band-edge energy levels within picoseconds, losing energy to heat. Large bandgap semiconductors generate little photocurrent due to poor absorption, while small bandgap semiconductors can suffer from low conversion efficiencies due to high thermalization losses. At the band-edge energy states, the electron–hole pairs can often survive for several microseconds before recombining, and they must be separated and transported to electrochemical interfaces for extraction during this time for effective energy conversion. This separation is assisted by the electric fields set up by charge distributions in the semiconductor and at the solid/liquid interface. Defects in the bulk and at the interface can adversely affect the separation fields, and also result in poor mobility for charge transport. If wide absorption widths are needed, for example, in indirect semiconductors (i.e., the absorber needs to be relatively "thick"), the charge transport losses can be severe. Thinner devices with back-surface optical reflection may reduce the loss.

To minimize overpotential loss due to interfacial charge extraction and electrochemical product formation, the interface conditions need to be optimized. Ideally, charge is extracted via the water-splitting half-reaction at the solid/liquid interface. The extraction process can be slowed or completely inhibited by poor energetic alignment or poor surface kinetics at the photoelectrode or counter electrode surfaces. Parasitic or corrosion reactions competing with the water-splitting reactions can also result in substantial loss; though surface treatments can be employed to kinetically and/or energetically favor water-splitting over the parasitic processes. Surface incorporation of nanoparticle catalysts is one approach, though light blockage due to such particles must be avoided. Since PEC water-splitting is a low-current density process, typically operating below 20 mA/cm^2, nonprecious metal catalysts can be used. Additionally, nanostructuring of electrode surfaces can increase effective surface area for enhanced charge extraction, although this can also lead to higher surface recombination loss.

The electrolyte is an important factor determining stability, efficiency of the charge-extracting reactions, and the electrochemical byproducts. Splitting seawater, for example, is a challenge since it is difficult to electrochemically suppress the production of chlorine gas from the Cl^- ions [71]. During PEC water-splitting, the evolved hydrogen or oxygen gas must be efficiently removed from the photoelectrode surface to avoid mass-transport losses in the surface reactions, and to minimize adverse optical effects. Surfactants added to the electrolyte have been successful in promoting rapid bubble formation and dissipation. In solution, ionic conductivity losses tend to be a larger problem. High electrolyte concentrations can be used to minimize this loss, but the tradeoff is in higher corrosivity.

Photoelectrode geometry and counter-electrode proximity are critical parameters to the redistribution of ions. In some geometries, gas separating membranes are needed, introducing further ionic transport loss.

Overall, the key condition for PEC hydrogen production is that the quasi-Fermi levels under solar illumination generate sufficient useable photopotential to drive the redox reactions for water splitting after all the solid-state, interfacial and solution overpotential losses have been taken into account. This challenge has severely limited efficiency in all single-junction PEC devices to date.

7.4.5 Single Junction Efficiency Limits

It is difficult to achieve high STH conversion efficiencies in single-junction PEC photoelectrode systems with inherent electrochemical and solid-state losses. Large bandgap semiconductor materials would be needed to generate sufficient useable photopotential. This, however, can severely limit photon absorption, therefore reducing photocurrent and STH conversion efficiency. The bandgap tradeoff between photopotential and photocurrent is particularly detrimental for single junctions. For example, if the minimum water-splitting potential, including the redox separation and overpotentials, amounts to 1.6 V, then the required quasi-Fermi level separation is also 1.6 eV. Even for high-quality semiconductor materials, the quasi-Fermi level separation can only achieve 50–70% of the bandgap level [72]. In this case, the minimum bandgap for the onset of photoelectrolysis would be 2.7–3.2 eV. For increasing levels of hydrogen production, the system losses will also increase, including the current-dependent surface overpotentials as well as electrical and ionic conductivity losses. Even higher bandgaps would then be required.

An upper bound for STH conversion efficiency can be established as a function of semiconductor bandgap based on fundamental optical absorption limits [50, 73]. Figure 7.15 plots the maximum attainable AM1.5G photocurrent densities in a semi conductor as a function of bandgap based on optimal light absorption and carrier extraction. The derivation assumes that every photon in the solar spectrum with an energy exceeding the bandgap will create an electron–hole pair, and that all of these electron–hole pairs are converted to photocurrent. For bandgaps greater than 3.2 eV, the photocurrent density is limited to approximately 1 mA/cm^2. This places an upper limit of 1.23% on the STH efficiency, as calculated using (7.4). The STH values corresponding to the maximum achievable photocurrents are listed in parentheses on the right vertical axis of Fig. 7.15, but these only apply to junctions capable of spontaneous water-splitting. Strictly speaking, any photoelectrode system incapable of sustaining photoelectrolysis will not produce photocurrent and thus have 0% STH efficiency.

Fundamental thermodynamic limits for the conversion efficiency of single- and multijunction semiconductor PEC devices have also been established in numerous studies [74–81]. The thermodynamic single-junction limit under ideal conditions, i.e., including thermalization losses but with no overpotential losses, has been

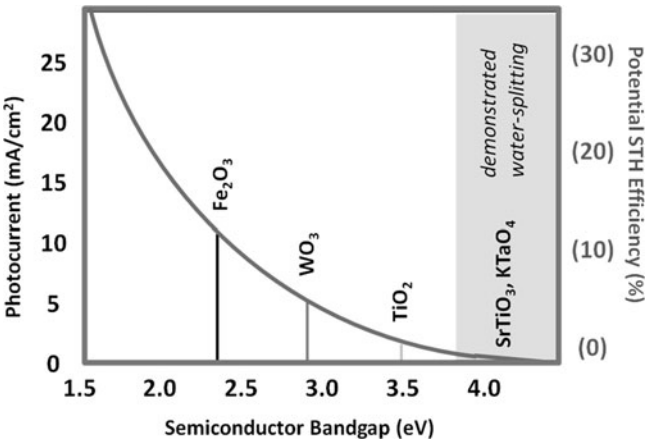

Fig. 7.15 Maximum achievable photocurrent density levels and potential solar-to-hydrogen conversion efficiencies for single-junctions as a function of bandgap based on optical absorption limits. Highlighted are the high-bandgap materials that have demonstrated spontaneous PEC water splitting but at correspondingly low efficiencies

calculated to be approximately 30% STH. With recovery of some thermalization losses through advanced multi-exciton device schemes, this limit is modestly increased to 32% STH [74]. More thorough analyses have been reported which include overpotential losses in addition to the optical and thermalization losses. These have indicated that the best single junction PEC cells for AM1.5G water-splitting will likely to be limited to STH efficiencies below 12%, even using the highest quality semiconductor and catalyst materials currently available [82].

7.4.6 Single Junction Examples

To date, the only demonstrations of single-junction water-splitting have utilized very high bandgap materials such as $SrTiO_3$ and $KTaO_4$ [83, 84]. Based on poor photon absorption, the demonstrated STH values have been well below 1%, consistent with the values in Fig. 7.15. Commonly studied semiconductor PEC materials have included iron oxide (Fe_2O_3), tungsten trioxide (WO_3), and titanium dioxide (TiO_2). The theoretically achievable photocurrent densities highlighted in Fig. 7.15 look encouraging, especially those for iron oxide. However, none of these materials can develop enough useable photopotential under sunlight to split water, not even the TiO_2 with a bandgap over 3.0 eV. To enhance the photopotential, these and other promising semiconductors can be incorporated in multijunction PEC schemes. This is consistent with the multijunction device enhancements that are well known in the PV community. For PEC devices, the same approach can be taken to enhance the photopotential and also to increase the absorption efficiency, as described in the following sections.

7.5 Multijunctions

Multiple-junction semiconductor devices for solar energy conversion are well-known, especially to the PV research community. The use of multijunction approaches for high photovoltaic conversion efficiency is the basis of current technologies for space applications, and one of the major cornerstones for future *Third Generation* PV devices [85]. In theory and practice, integration of multiple junctions in stacked solar cells enhances the absorption of photons in the solar spectrum [64, 85, 86]. In fact, multijunction III–V solar cells with efficiencies greater than 40% are commercially available [87, 88]. Efficiencies in PEC solar conversion devices can also be enhanced by improved spectral absorption in multijunction configurations. More importantly, multijunction PEC devices can develop increased photopotentials, better meeting the voltage demands of water splitting. The tradeoffs are reduced photocurrent, which adversely affects hydrogen production rates, and added device complexity. Overall, a PEC multijunction device design must strike the right balance to maximize STH conversion efficiency without adding too much cost. The multijunction approach, with its benefits, limitations, and tradeoffs are further discussed in the following sections.

7.5.1 Multijunction Stacks

The concept of stacking multiple photorectifying cells is illustrated in Fig. 7.16. Though the figure specifically depicts a triple cell stack, the illustration can be generally extended to represent any number of stacked cells. Each cell in the stack represents an independent photoconverting junction, such as a semiconductor *pn junction*, or a semiconductor/electrolyte PEC junction. Electrically and optically the cells are stacked together in a series-connected fashion. Incident sunlight on the "top" cell is partially absorbed, generating a photovoltage and photocurrent in the process. The remaining filtered light reaches the "middle" cell, where further absorption and photoconversion takes place. Any remaining sunlight can be absorbed and converted in the "bottom" cell. Since the cells are series-connected, the individual photovoltages will add, but the net current will be the minimum of the individual cell photocurrents. This is because the net current through the device must be continuous, and will be bottlenecked by the minimum component cell current. Any excess carrier generation in the other cells will be lost internally to recombination. Since the individual cells are all powered by some fraction of the incident solar photons, particularly the buried cells, they operate at reduced photocurrents compared with full-sun levels. As a result, overall device current is reduced by the bottleneck effect. Typically, then, a multijunction device based on a given semiconductor material system will generate lower photocurrent compared with a single-cell device of the same material. In general, multijunction devices offer higher voltage with lower current. As illustrated in later sections, over-all conversion efficiencies can be enhanced due to the extended range of photons effectively absorbed using multiple bandgaps in an integrated device.

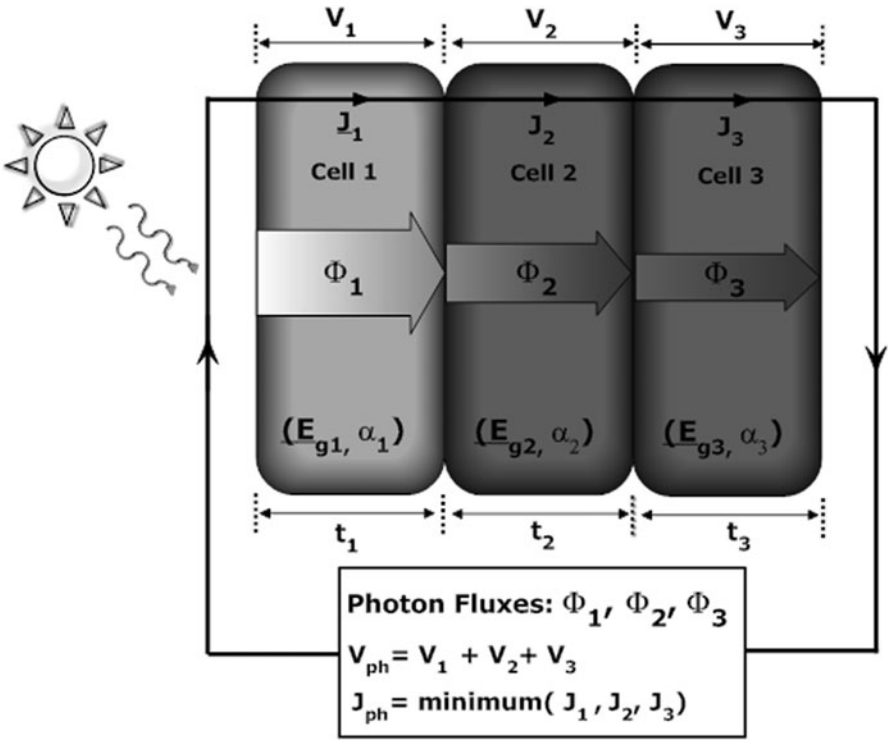

Fig. 7.16 General schematic of a three-cell stack of three absorber materials with bandgap E_g and absorption coefficient α. Indicated are the photon fluxes in each cell (Φ), along with the generated photovoltages (V) and photocurrent densities (J). The total voltage in the series-connected stack is the sum of the individual cell voltages, while the stack current is the minimum of the individual cell currents

7.5.2 Optical Considerations

Semiconductor photorectifying cells absorb photons in the solar spectrum, and can convert some of the absorbed photon energy into electricity or chemical products, such as hydrogen. Different semiconductors are specifically sensitized to different parts of the solar spectrum dependent on optoelectronic properties related to bandgap and absorptivity. In general, the macroscopic light absorption process in a material follows the Beer–Lambert Law [89], here expressed as a function of photon wavelength, λ:

$$I_\lambda(x) = I_{0,\lambda}\, \mathrm{e}^{-\alpha_\lambda x}. \tag{7.8}$$

For each photon wavelength λ in (7.8), $I_{0,\lambda}$ is the intensity of the incident flux (e.g., in W/m^2), α is the absorption coefficient (in m^{-1}), and x is the length of the optical pathway through the material (in m). I_λ is the unabsorbed flux intensity emerging out the back of the material, as illustrated in Fig. 7.17.

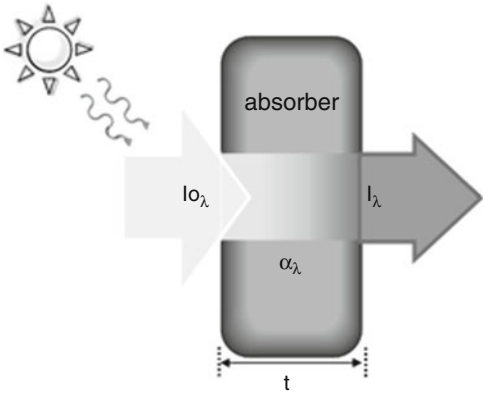

Fig. 7.17 Illustration of the Beer–Lambert Law for wavelength-dependent photon absorption in a material with absorption coefficient α

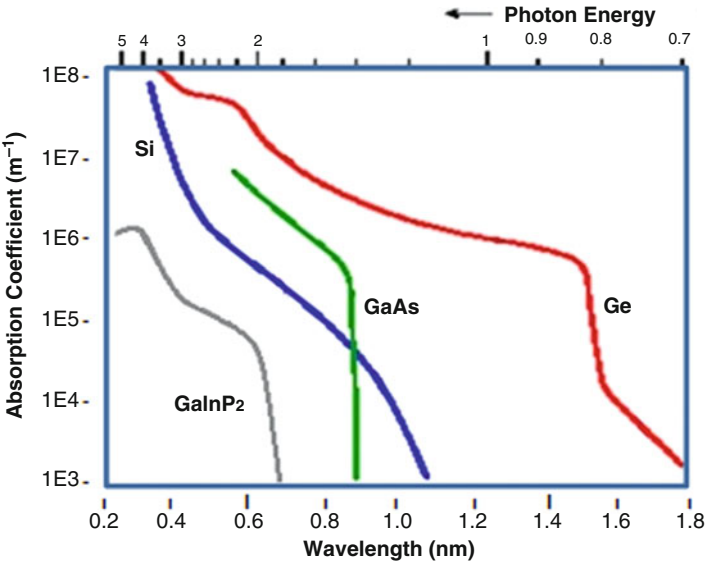

Fig. 7.18 Absorption coefficient spectra of $GaInP_2GaAs$, Ge, and Si

Important information about the spectral-sensitivity of a given semiconductor material is incorporated in the absorption coefficient α, which is strongly dependent on material bandgap and allowable energy transitions. Figure 7.18, for example, depicts typical absorption coefficient curves for four different crystalline semiconductors: (1) gallium indium phosphide ($GaInP_2$), a direct band transition semiconductor with bandgap 1.86 eV (corresponding to a photon wavelength of 667 nm); (2) gallium arsenide (GaAs), a direct band transition semiconductor with

bandgap 1.43 eV (868 nm); (3) germanium (Ge), an indirect transition material with bandgap 0.66 eV (1,880 nm); and (4) silicon (Si), an indirect transition material with bandgap 1.12 eV (1,110 nm). For all four cases, the absorption coefficient vanishes at the gap energy, consistent with nonabsorption of photons with energies below the bandgap.

For photons with energies above the bandgap, the direct transition materials absorb more efficiently. This is reflected in the steeper slopes and correspondingly higher values for α in $GaInP_2$ and GaAs near their band energies, specifically compared with Ge and Si. Solar energy conversion devices based on direct-transition materials such as GaAs can be made as thin as a few micrometers and still absorb most of the available photons. In contrast, silicon solar cells need to be made much thicker, typically 100 μm or more to absorb most of the sunlight. A key point relevant to multijunction device design is that photon absorption and photocurrent generation in the individual component cells can be tailored by the selection of semiconductor bandgap and absorption properties. They can also be adjusted by varying cell thickness, as indicated in the Beer–Lambert law.

Another important parameter describing the optoelectronic response in a photoactive semiconductor device is the *quantum efficiency* (QE) (more precisely, the external quantum efficiency or EQE), which is critical to both single- and multijunction device designs. For each wavelength of light, the "external" QE expresses the percentage of photons incident on the device surface that results in an extracted electron–hole pair. This parameter is therefore an accurate measure of the device's ability to generate photocurrent, and convert solar energy. The QE ratio and the corresponding relationship to photocurrent generation in a given semiconductor device can be expressed as:

$$\mathrm{QE} = \frac{\#\mathrm{charges/s}}{\#\mathrm{photons/s}} = \frac{I/e}{P_{\mathrm{total}}(\lambda)/E_{\mathrm{photon}}(\lambda)}, \tag{7.9}$$

where e is the elementary charge, I is the current, $P_{\mathrm{total}}(\lambda)$ is the total power of incident light at a wavelength λ, and $E_{\mathrm{photon}}(\lambda)$ is the energy of a single photon at wavelength λ.

The quantum efficiency is closely related to the absorption coefficient, but incorporates additional information regarding the efficiency of extracting photocharges created in the absorption process. Figure 7.19 shows representative QE spectra for $GaInP_2$, GaAs, and Ge devices, with sensitized regions of the AM1.5G included above. It is evident that the different semiconductors are sensitized to specific portions of the solar spectrum. Ge exhibits a broad bandwidth in its spectral sensitivity, but there is a relatively low level of solar photon flux across this bandwidth. In contrast, both $GaInP_2$ and GaAs have more narrow bandwidths, but each is efficient at converting photons in high-flux portions of sunlight. It is important to emphasize that QE is dependent not only on absorption and charge separation properties of device, but also on device operating conditions, such as voltage biasing, which alter

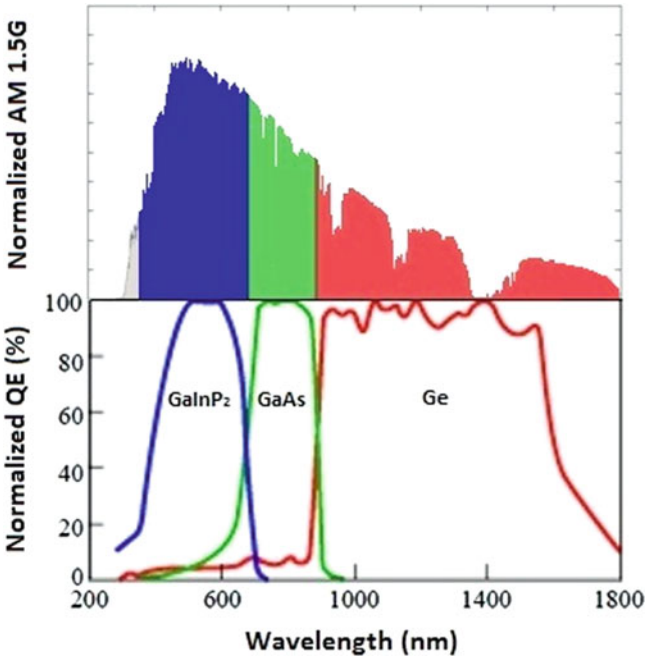

Fig. 7.19 Normalized QE curves of $GaInP_2$, GaAs, and Ge shown with the regions of spectral absorption for each material highlighted in the AM1.5G spectrum above

charge distributions and electric fields. These operating conditions need to be specified in reported QE curves to be useful in device design.

The solar energy conversion in a single bandgap semiconductor device is ultimately limited by the spectral width of the quantum efficiency curve. Also, since photogenerated electron–hole pairs rapidly thermalize to near band-edge energy states, energy conversion is most efficient for near-bandgap wavelengths. Absorbed photons with energies in excess of the bandgap will lose this excess to thermalization, reducing the conversion efficiency of light at the corresponding photon wavelength. Referring to the QE curves in Fig. 7.19, individual $GaInP_2$, GaAs, and Ge devices, for example, can convert photons in the 300–700, 700–900, 900–1,800 nm ranges, respectively, with optimal conversion near the 667, 868, and 1,800 nm bandgaps, respectively. By extension, a triple-junction stacked device using all three materials could absorb over a broader range of wavelengths from 300 to 1,800 nm, with optimal conversion efficiency at all the component cell bandgaps of 667, 868, and 1,800 nm. This illustrates an important avenue for enhanced efficiencies in multicell device schemes, relevant to both PV and PEC systems. The strategy has been studied extensively in the PV research and development community, and "full spectrum" absorber devices based on stacked multiple junctions are

envisioned as a future pathway to ultrahigh solar-to-electric conversion efficiencies [90]. As discussed in following sections, photovoltaic efficiencies in triple-junction III-V devices have already exceeded 40%.

7.5.3 Current and Voltage Relationships

The external quantum efficiency spectrum indicates the efficiency of photogenerated charge extraction and current generation as a function of photon wavelength. The QE specified at the device operating condition coupled with the incident photon flux provide sufficient information for determining the photocurrent of the device. Specifically, the theoretical carrier extraction rate is determined by integrating the product of QE and flux over the light spectrum. The photocurrent density is then equal to the extraction rate scaled by the ratio of electron charge/photon energy. The photocurrent equation can be explicitly written as an integral over photon wavelengths in the incident irradiation:

$$J_{\mathrm{ph}} = \int_{\mathrm{irradiance}} \Phi_{\lambda} \left(\frac{e\lambda}{hc} \mathrm{QE}_{\lambda} \right) \mathrm{d}\lambda. \tag{7.10}$$

In (7.10), J_{ph} is the photocurrent density (e.g., in A/m^2 or mA/cm^2) at device operating conditions, h is Planck's constant, and c is the speed of light. Wavelength-dependent parameters include the incident irradiance flux, Φ_{λ}, and the quantum efficiency, QE_{λ}, which is specified at the operating conditions.

As an example of J_{ph} determination from QE and solar flux, Fig. 7.20 illustrates the QE response at short-circuit conditions for a typical monocrystalline silicon PV single-junction cell along with the corresponding responsive regions of the AM1.5G spectrum. Integrating QE according to (7.10) using AM1.5G as the input irradiance yields 35 mA/cm^2, consistent with the short-circuit photocurrent levels of commercial single-junction silicon PV devices [64]. As seen in Fig. 7.20, silicon, with a bandgap of 1.12 eV, has a broad spectral response for absorbing sunlight. Efficient energy conversion with low thermalization loss in this single-junction device, however, is limited to absorbed photons with energies near the bandgap energy (wavelengths near 1,100 nm). As a result, compared with the PV efficiencies exceeding 40% in multijunction III–V devices, efficiencies are limited to about 20% using single-junction silicon.

The useable photovoltage (equivalently, the photopotential) generated in a semiconductor device under illumination can be represented by the split in the quasi-Fermi levels as described in Sect. 7.4. This voltage is a function of semiconductor bandgap, but it is always less than the internal energy separation between conduction and valence bands represented by the bandgap. In PV cells, the maximum useable potential, expressed by the open-circuit voltage, is typically 50–70% of the bandgap energy [64, 91]. For example, silicon has a bandgap of 1.1 eV, and

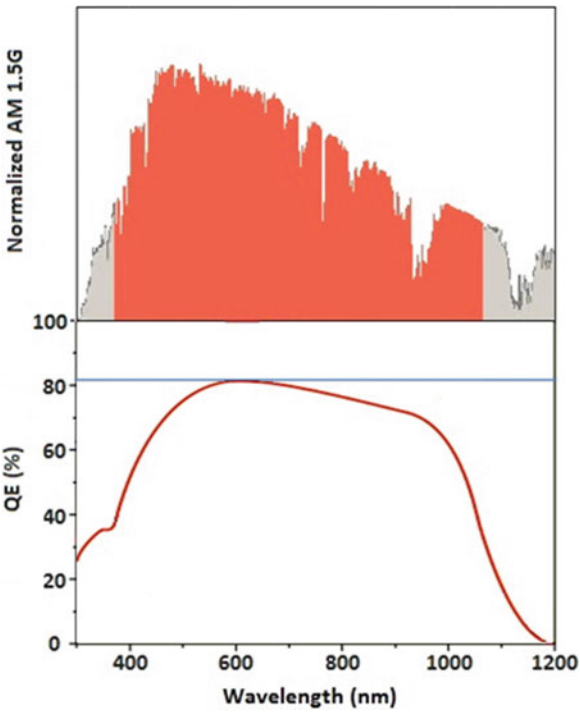

Fig. 7.20 QE curve of a typical monocrystalline silicon solar cell the region of spectral absorption for the device highlighted in the AM1.5G spectrum above

typical open circuit voltages of single junction crystalline silicon cells are around 0.6 V. Similarly, high-quality GaAs has a bandgap of 1.4 eV, and device open circuit voltages of approximately 1.0 V. As the photoconversion device is asked to deliver current to an external load, the operating voltage will start to decrease below the maximum potential. The photovoltage and photocurrent levels are integrally related. Specifically, the maximum photovoltage is logarithmically related to the current-generating capability of the device, as derived from junction analysis [64, 92]. For photovoltaic cells, this is expressed as a relationship between the open-circuit voltage, V_{oc}, and the short-circuit current-density, J_{sc}:

$$V_{oc} = V_T \ln\left(\frac{J_{sc}}{J_0} + 1\right), \tag{7.11}$$

where V_T is the temperature-dependent thermal voltage of the device, and J_0 is the device's saturation current density.

The current and voltage relationships coupled with the optical parameters described in the previous section for single material systems provide powerful insights into the voltage, current, and conversion efficiency properties of single junctions, and also of stacked semiconductor device configurations. Another important performance parameter representing the quality of photorectifying junctions is the "fill factor," or FF. The FF expresses how severely voltage will drop below the maximum useable potential under current loading. This is illustrated in Fig. 7.21, showing photoconversion device performance curves with "good" and "poor" fill

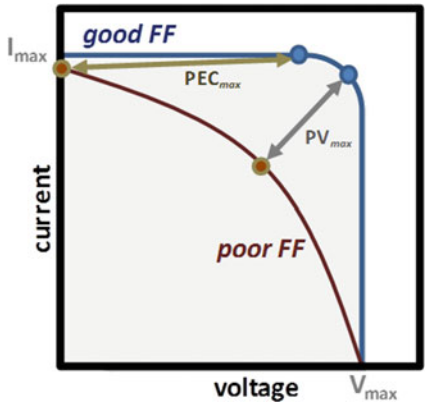

Fig. 7.21 Current/voltage response curves of photoconversion devices with good and poor fill factors (FF), showing maximum voltage, current, and power points for each curve

factors. In PV cells, the maximum power point, found at the "knee" of the performance curve, is greatest for high fill factors. For PEC hydrogen production cells, it is necessary to maintain a high photopotential to drive the water splitting reactions while maintaining high photocurrent to maximize production rates. In other words, it is desirable to operate a PEC cell at maximum possible current with minimum voltage drop below the device's maximum useable potential. A good fill factor is also critical in this situation. A high solar conversion efficiency in PV and PEC devices requires material systems and devices with maximum-photovoltage, maximum-photocurrent and fill factor all optimized.

The current and voltage relationships for individual single-junction cells can be combined to model of multijunction devices. The generic triple-junction scheme shown in Fig. 7.16, for example, can be modeled by the set of equations summarized in Table 7.1. These equations specifically highlight the dependencies of device photovoltage and photocurrent on the individual cell absorption coefficients and quantum efficiencies. This multijunction equation set is explicit to a three-cell device, but readily generalized to devices with any number of stacked cells. Additionally, the relationships expressed are applicable whether the individual cell junctions are photovoltaic, PEC, or a combination. If the device stack is designed to generate electricity, the PV conversion efficiency is determined at the "maximum power point," as illustrated in the response curves of Fig. 7.21. Conversely, if the stack is designed to utilize solar energy for purposes of splitting water, the PEC conversion efficiency depends on the maximum achievable electrochemical photocurrent. In either case, optimizing voltage, and even more importantly, maximizing current is desirable for achieving high efficiency. Some key take-away points from the relationships in Table 7.1 relating to multijunction device design and optimization include the following:

- *Photocurrents are decreased in multijunctions*
  - Photocurrent in a component cell is dependent on the physical and optoelectronic properties of that cell, such as thickness, bandgap, and QE, but also on the available photon flux.

Table 7.1 System of equations relating voltage, current, and spectral responses in photoconversion cells and stacks

	Cell 1	Cell 2	Cell 3
Absorber bandgap (E_g) (eV)	E_{g1}	E_{g2}	E_{g3}
Thickness (t) (μm)	t_1	t_2	t_3
Absorption coefficient (α) (μm^{-1})	$\alpha_1(\lambda)$	$\alpha_2(\lambda)$	$\alpha_3(\lambda)$
Photon irradiance (Φ) ($mW/cm^2/nm$)	$\Phi_1 = 1$ sun	$\Phi_2 = \Phi_1 e^{-\alpha_1 t_1}$	$\Phi_3 = \Phi_2 e^{-\alpha_2 t_2}$
Spectral response (CR) (C/J)	$SR_1 = \frac{q}{E_g(\lambda)} QE_1$	$SR_2 = \frac{q}{E_g(\lambda)} QE_2$	$SR_3 = \frac{q}{E_g(\lambda)} QE_3$
Short-circuit current (J_{ph}) (mA/cm^2)	$J_{ph1} = \int_{\lambda g1}^{\infty} \Phi_1 SR_1 \, d\lambda$	$J_{ph2} = \int_{\lambda g2}^{\lambda g1} \Phi_2 SR_2 \, d\lambda$	$J_{ph3} = \int_{\lambda g3}^{\lambda g2} \Phi_3 SR_3 \, d\lambda$
Open-circuit voltage (V_{oc}) (mV)	$V_{oc1} = V_T \ln\left(\frac{J_{sc1}}{J_{01}} + 1\right)$	$V_{oc2} = V_T \ln\left(\frac{J_{sc2}}{J_{02}} + 1\right)$	$V_{oc3} = V_T \ln\left(\frac{J_{sc3}}{J_{03}} + 1\right)$
Total device V_{oc}	$V_{oc} = V_{oc1} + V_{oc2} + V_{oc3}$		
Total device J_{ph}	Minimum (J_{ph1}, J_{ph2}, J_{ph3})		

  - Photon flux available to a component cell is filtered, therefore reduced, by absorption in preceding cells in the stack. This optically couples photocurrent generation in all the cells.
  - The output current of the stack is limited to the smallest of the photocurrents produced by any of the constituent cells, and optical coupling effects between cells become important in device design.

- *Photovoltages are enhanced in multijunctions*
  - Photovoltages of the components cells are additive in the stacked device, providing higher useable photopotential.
  - Photovoltage in a component cell is logarithmically dependent on the photocurrent, so current reduction due to filtering will decrease voltage, but not significantly.

- *Optics are important*
  - Available flux in a component cell is determined by light absorption in previous cells, but light reflection is also important. Minimizing reflection at the front surface and at each interface while maximizing back-surface reflections to redirect light back through the device can significantly enhance efficiency.

- *Fill factor is important*
  - Although fill factor is not represented explicitly in the equation set, optimal fill factor is important in each cell to ensure maximum output photocurrents with minimal loss in photovoltage.

Using these general points as guidelines, it is possible to develop practical designs for highly efficient multijunction devices. There are still a number of general design challenges for practical implementations that need to be considered.

7.5.4 General Design Challenges

In effective designs, maximum current in a multijunction photoconversion device is achieved by "current-matching" the individual cells in the stack [93]. For current-matching, the component cell materials and thicknesses can be tailored to ensure all component cell photocurrents are approximately the same. The goal is to minimize internal current losses. Since current must be continuous across the entire device, the lowest component cell photocurrent will bottleneck the output. If current excess is generated in any of the other component cells, it will be lost through internal recombination. If all junction currents are the same, this recombination loss is minimized, and net current is maximized. As an alternative viewpoint of current matching, the cells in the stack are essentially "splitting" all of the incident solar energy photons that can be used for photocurrent generation. Again, since the cell with the lowest current dictates the device current, an equal split will be optimal. Since photocurrent generation is sensitive to the incident flux of photons as well as physical and optoelectronic properties of all the cells, the process of designing an optimal current-matched device is complex. A general approach involves stacking semiconductors with decreasing bandgaps. Top layers absorb higher energy photons while transmitting lower energy photons that are subsequently absorbed by following layers of the device. After a component cell's bandgap and quantum efficiency have been established, cell thickness can be adjusted to alter the number of absorbed photons, and tune the photocurrent.

An important challenge in the design of multijunction devices is the limited selection of availability of semiconductor materials with appropriate bandgaps that offer high efficiency through low defect densities. Examples of PV material systems that have been successful or have shown promise for multijunction configurations include the III–V crystalline materials, amorphous hydrogenated silicon films, and copper chalcopyrite thin-films [86, 94, 95]. In each case, bandgap tuning is available through modification of alloy composition. A broader class of low-cost thin-film PEC material systems for multijunction water-splitting applications is under investigation, including novel metal oxides and oxi-nitride compounds covering a broad range of bandgaps [96–99]. In the PEC junction case, there are additional material challenges associated with the potential and band-edge requirements for water splitting, as well as stability in solution.

In addition to the material selection challenge, interface design for low optical and defect recombination losses in stacked cells is complicated, and highly dependent on the materials being interfaced. In crystalline semiconductor multijunction devices, lattice-matching between adjacent layers is critical for avoiding defects and significant interfacial recombination losses [100, 101]. In polycrystalline and

amorphous thin film material systems, stress and strain at the various film interfaces must be minimized to avoid defects and even possible delamination of the device. In semiconductor material systems where heavy doping can be readily achieved, thin "tunnel junctions" are the preferred method of forming low-loss connection between adjacent cells [101]. Precise process control is essential in successful tunnel junction implementations. In other material systems where tunnel junction formation is not possible, the use of conductive transparent oxides can be used to interface adjacent cells, but optical and contact resistance losses can be introduced. To retain the efficiency advantages of multijunctions, all interface losses need to be minimized.

Broader challenges exist in the processing and manufacture of monolithic multijunction designs. In crystalline, polycrystalline, and amorphous semiconductor processing, precisely controlled process conditions are essential to the formation of device quality materials; and these conditions are highly material specific. Developing a process sequence to successfully stack numerous semiconductor layers can be extremely difficult. During the process, fabrication conditions at later stages, particularly high-temperature processes, can adversely affect the quality of all preceding layers. Low temperatures are advantageous for process compatibility and for lower manufacture cost, but it is often difficult to obtain the necessary material quality. The trade-offs boil down to enhanced performance vs. added complexity and manufacture cost. In PEC water-splitting applications, the increased photopotentials developed in multijunction devices is an added benefit to the mix. In the PV industry, the multijunction approach has been a clear winner in applications when the highest conversion efficiencies are absolutely required, despite higher cost.

7.5.5 Photovoltaic Multijunctions

The multijunction approach for achieving enhanced conversion efficiencies in PV devices have been studied for several decades. Since the early 1980s, solar-to-electric conversion efficiencies in production scale multijunction PV cells have been increased from just over 15% to over 40% today [86, 102]. The most efficient present-day multijunction photovoltaic cells are based on high-quality, and high cost, crystalline III–V material systems. For example, commercial cells have been on the market for several years, primarily for space applications, utilizing the $GaInP_2$, GaAs, and Ge materials discussed in Sect. 7.5.2. These specific materials were selected based on their collective ability to absorb photons over a broad range of the solar spectrum, as was seen in Fig. 7.19. $GaInP_2$, with a bandgap energy of 1.85 eV, absorbs short wavelength ultraviolet and visible photons in the solar spectrum; GaAs, with a bandgap of 1.42 eV, absorbs near-infrared light; and Ge, with a bandgap of 0.67 eV absorbs the lower energy photon energies in the infrared. In the device fabrication process, layers of crystalline GaInP, GaAs, and Ge layers are monolithically grown on a Ge substrate using epitaxial methods [103]. The completed triple-junction device scheme, containing over 20 layers, is illustrated in Fig. 7.22.

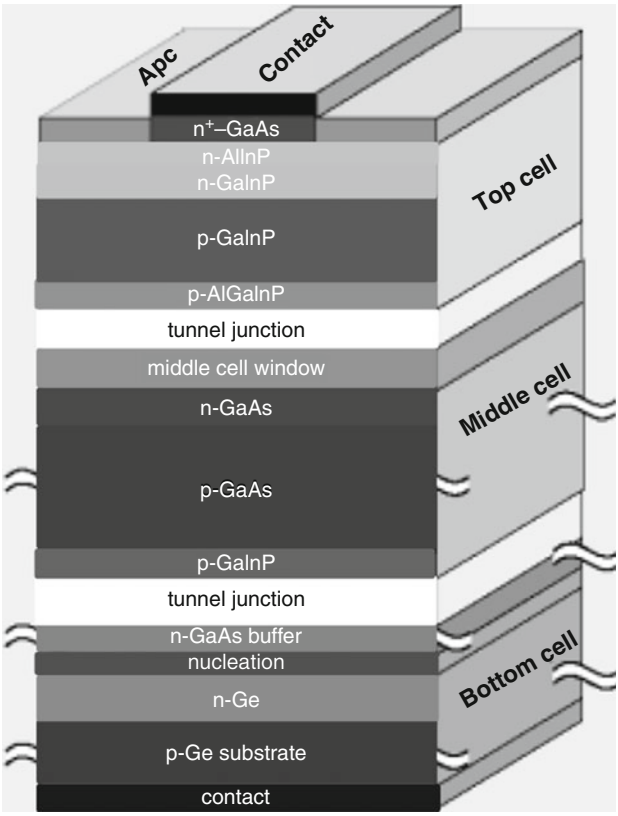

Fig. 7.22 Device structure of a high efficiency $GaInP_2$/GaAs/Ge triple-junction solar cell developed at NREL and commercialized by Spectrolab

Several critical design features were necessary to enable high performance in these devices. For example, current matching among all three component cells was essential for maximizing photocurrent output. To avoid losses due to interface defects, the semiconductor layers in this configuration had to be lattice matched. Additionally, low-loss electrical contact between adjacent cells was achieved using optimized tunnel junctions, comprised of a ministack of highly doped layers producing an effective potential barrier for both minority carriers. Furthermore, a broadband dual-layer dielectric stack antireflection coating was employed. The resulting multijunction device achieves PV efficiencies over 34% under concentrated sunlight [104]. More recent variations on the device scheme utilizing a $Ga_{0.44}In_{0.56}P/Ga_{0.92}In_{0.08}As$/Ge stack have achieved over 40% PV efficiency under concentrated sunlight with open-circuit voltages over 3.0 V and operating voltages near 2.75 V [87]. These efficiencies represent world records in the field of photovoltaic solar energy conversion, but this comes at a price. The crystalline III–V material systems are prohibitively expensive, especially for any large-scale deployment.

As a lower cost alternative, multijunction devices incorporating thin-film semiconductors have also been developed. As an example, triple junction thin

film solar cells based on amorphous silicon/germanium alloys have been developed with photovoltaic efficiencies over 10% and with open-circuit voltages up to 2.3 V [54]. The fundamental design strategies for optimizing efficiency in these lower cost devices are similar to those in the III–V designs, including current matching, tunnel junction optimization, and minimization of optical losses. In a typical device, the thin-film silicon–germanium alloy bandgaps are adjusted to approximately 1.8, 1.55, and 1.4 eV in the top, middle, and bottom cells, respectively, to achieve current matching and broad spectral response. Also in the design, front-surface antireflection coatings are incorporated, while back surface reflector layers are used to reflect photons back into the device. Compared with single-junction devices using amorphous silicon–germanium material systems, the multijunction approach fully utilizes more of the solar spectrum. Higher conversion efficiencies are therefore achieved, but again at the expense of added device complexity and cost. Rigorous efforts in loss minimization are critical to ensure that the enhanced performance in the PV multijunctions offer worthwhile advantages over simpler single-junction devices. Efforts to achieve even higher efficiencies in economical thin-film multijunction technologies are on-going; not only in amorphous silicon devices, but also in alternative, enhanced absorbers based on bandgap-adjustable copper chalcopyrite alloys. Similar efforts are also underway to develop efficient multijunction water-splitting PEC schemes incorporating a broader class of low-cost semiconductor materials, such as metallic oxide alloys. Additional design considerations apply in the PEC case.

7.5.6 PEC Multijunction Design Considerations

Multijunction device designs can combine PV cells to improve solar-to-electricity conversion efficiency, or they can incorporate a combination of PV and PEC cells to enhance solar hydrogen production via water splitting. In both cases, the stacked junctions can be beneficial, providing photovoltage enhancement, as well as the broadened solar absorption width. The primary tradeoff is added device complexity and cost. In the PEC case, an additional tradeoff is reduced photocurrent, which limits hydrogen production rates. To make multijunctions worthwhile, the PEC device design must strike the right balance to maximize conversion efficiency and minimize expense. The general design considerations discussed in preceding sections still apply, including current matching and interface loss minimization. There are, moreover, additional considerations specifically applicable to a PEC component cell, which could be incorporated into a multijunction stack as photoanode (OER electrode) or a photocathode (HER electrode). These considerations include the following:

1. Low loss semiconductor PEC electrode materials with appropriate bandgap, absorption properties, and device quantum efficiency are needed for efficient photon absorption and charge extraction.
2. Sufficient useable potential must be developed (i.e., overall split in quasi-Fermi levels for holes and electrons) across the stack under illuminated operating

conditions to overcome overpotential losses and drive the OER and HER reactions.
3. Suitable band-edge position at the semiconductor/electrolyte interface need to be established to facilitate the proper alignment of the quasi-Fermi levels under illumination.
4. High surface activities for the OER/HER reactions need to be established to minimize the interface overpotential losses.
5. High surface passivation, based on energetics and/or kinetics, needs to be established to mitigate corrosion and all other parasitic reactions.
6. There needs to be enough flexibility in selection of semiconductor bandgap, absorption properties and thickness to allow for current-matching in the stack design.
7. Losses associated with electrolyte conductivity and oxygen/hydrogen product gas management (related to relative electrode placement, ionic pathways between electrodes, possible membrane separators, and other related design features) need to be minimized.

Design optimizations, for all the component cells and for the integrated stack, are essential for realizing enhanced efficiency in multijunction devices. Decades of research and development in PV multijunctions has resulted in solar-to-electric conversion efficiencies exceeding 40% in triple junctions, approaching theoretical limits. In contrast, PEC multijunction research is at a far less mature level. Though STH conversion efficiencies exceeding 10% have been demonstrated in best PEC tandem devices based on high-quality III–V crystalline semiconductor materials, these "First Generation" devices lack long-term stability and affordability. More stable and affordable "Second Generation" thin-film PEC multijunction devices have been demonstrated, but only in the 3–5% STH range of performance levels. The following section examines the theoretical limits for any "First-," "Second-," or even "Third-" Generation multijunction systems, with specific emphasis on attainable STH efficiency.

7.5.7 Multijunction Efficiency Limits

As with the single-junction PV or PEC devices, efficiency bounds can be placed on multijunction configurations based on optical absorption limits. Figure 7.23 is a two-dimensional extension of Fig. 7.15 for tandem devices, where maximum photocurrent, and the corresponding STH levels for PEC devices, are calculated as a function of both top- and bottom-junction bandgaps. The assumptions included in the derivation of this graph are as follows:

1. The top cell absorbs all photons with energies exceeding the top-cell bandgap.
2. The bottom cell is illuminated with the top-cell-filtered light, and absorbs all of the remaining photons with energies exceeding its bandgap.

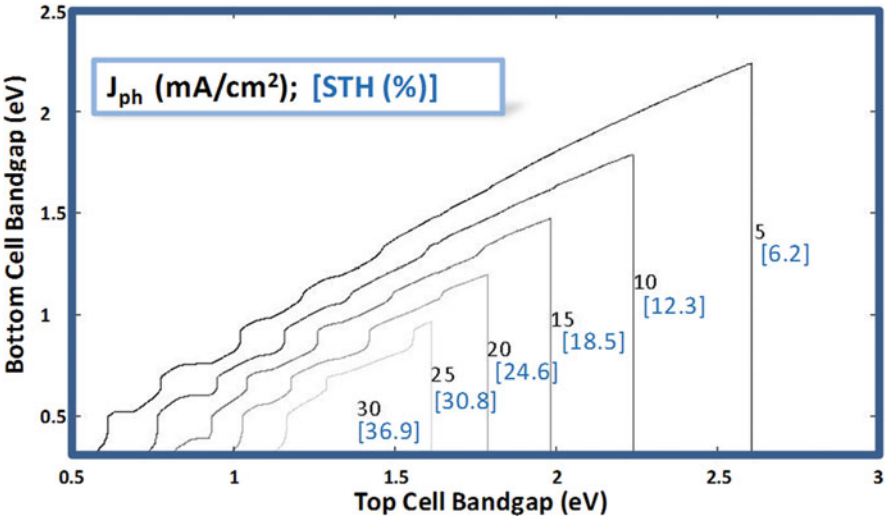

Fig. 7.23 Maximum achievable photocurrent densities in tandem semiconductor devices as a function of top and bottom cell bandgaps based on theoretical optical absorption limits. Included in brackets are the corresponding PEC STH efficiencies achievable in devices capable of water splitting

3. For every photon absorbed, an electron–hole pair is generated and extracted as photocurrent.
4. The total photocurrent of the stack is then simply the smaller of the two photocurrents produced by each individual cell.
5. For the case of PEC cells, the STH efficiencies, indicated in brackets in the plot, are calculated using (7.7), These ONLY apply to systems with sufficient photopotentials to split water.

The results from Fig. 7.23 are definitely encouraging for the viability of tandem photovoltaic electricity production as well as PEC hydrogen production. Despite the reduced photocurrents inherent in the tandem arrangement, a wide range of bandgap combinations yield high enough photocurrents for STH conversion efficiencies over 10%. An important key is to identify the possible bandgap combinations capable of the necessary photopotential levels for water splitting. The useable potential of a single cell ranges from 50 to 70% of the semiconductor bandgap, with 70% achievable only in the highest quality materials. In addition, the tandem device photopotential needs to exceed the water-splitting potential in addition to overpotentials, typically requiring around 1.6 V. The combined bandgap of the two component semiconductor materials would then need to be somewhere between 2.3 and 3.2 eV, with the high end of the range for most materials, and the low end only for the highest quality materials. There are many pitfalls and extra losses in real-world multijunction implementations, so the general rule is no guarantee of successful water splitting.

It is important to emphasize that even if the tandem device develops sufficient potential to split water, the STH efficiency will always be restricted based on the lowest photocurrent in the stack, usually in the highest bandgap cell. As an illustration, TiO_2 with bandgaps of 3.1 eV could be combined with a low bandgap semiconductor such as silicon (1.1 eV) in a hybrid tandem to meet the photopotential requirement for PEC water splitting. As seen in Fig. 7.17, however, independent of the bottom junction, the device performance will never exceed approximately 2.5% STH. In this example, and in any series-connected tandem configuration, the performance is bound by the photocurrent limits of the highest bandgap PEC semiconductor. As an alternative hypothetical example for achieving STH efficiencies above 10%, a high-quality top cell semiconductor with a bandgap of 2.0 eV can be coupled with a 1.0 eV semiconductor for the bottom cell. This combination satisfies the combined bandgap requirement, and is within the 12–19% STH range, in fact, approaching 19% as seen in Fig. 7.23.

As discussed in Sect. 7.3.1, fundamental thermodynamics limits conversion efficiency for both single- and multijunction semiconductor PEC devices have also been established in numerous studies. The thermodynamic tandem limit under ideal conditions, i.e., including thermalization loss, but with no overpotential loss, has been calculated at approximately 40% STH. This is consistent with the optical limits shown in Fig. 7.23. It is also substantially higher than the 30% STH limit established for the single-junction case. Moreover, employing advanced multi-exciton device schemes which eliminate part of the thermalization loss, the theoretical tandem limit is further increased to 46% STH [58].

As also discussed in Sect. 7.3.1, more detailed analyses of multijunction PEC devices including optical, thermalization, and overpotential losses have been reported. Figure 7.24 shows the maximum achievable photocurrent density and possible associated STH conversion efficiency results from the Rocheleau and Miller analysis [82] for tandem devices of high-quality III–V semiconductors. This analysis, which focuses on devices operating in the high-efficiency region seen in the optical limits plot of Fig. 7.23, includes estimates for solid-state and electrochemical losses. As expected, the STH efficiency limits are somewhat lower than the optical limits, though they still do exceed 25% over a limited range of top and bottom cell bandgaps. The high-quality factor of the modeled semiconductors clearly plays a large role in maintaining high levels of performance. For lower quality thin-film materials, larger efficiency hits would be expected. Nevertheless, there should be adequate margins for achieving over 10% in thin film tandem devices under some circumstances [82].

As an illustration of this, the analysis of efficiency limits for triple junctions based on lower quality amorphous silicon materials were also reported by Rocheleau and Miller. In that analysis, a bottom cell, with a bandgap of 1.45 eV was assumed, and the middle and top cells were modeled based on the available range of bandgaps in thin-film silicon materials. The resulting current density and STH efficiency limits are shown in Fig. 7.25. Interestingly, even with the lower quality thin film materials, and despite the further photocurrent limits in the triple junction case, STH efficiencies in the 10–13% STH range appear readily attainable.

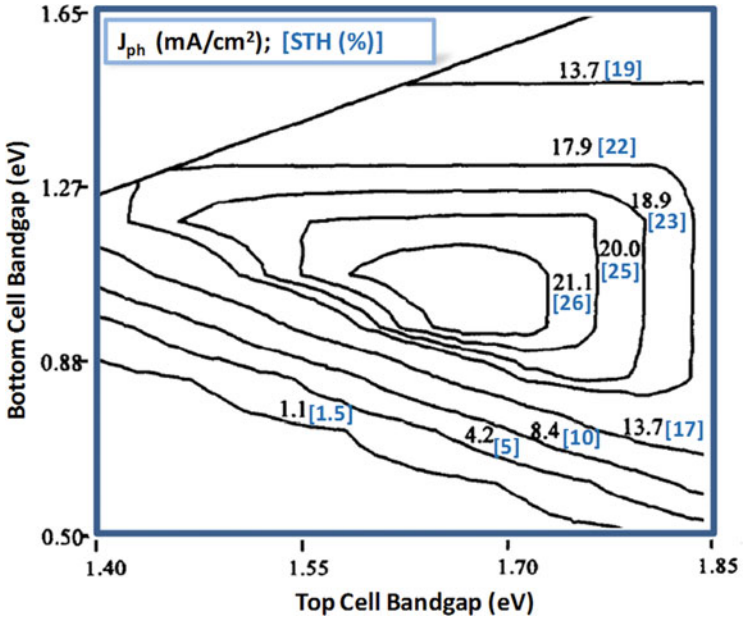

Fig. 7.24 Maximum achievable photocurrent densities and PEC STH efficiencies in tandem III-V semiconductor stacks as a function of top and bottom cell bandgaps based on analyses of Rocheleau and Miller [82] which included solid-state and electrochemical losses

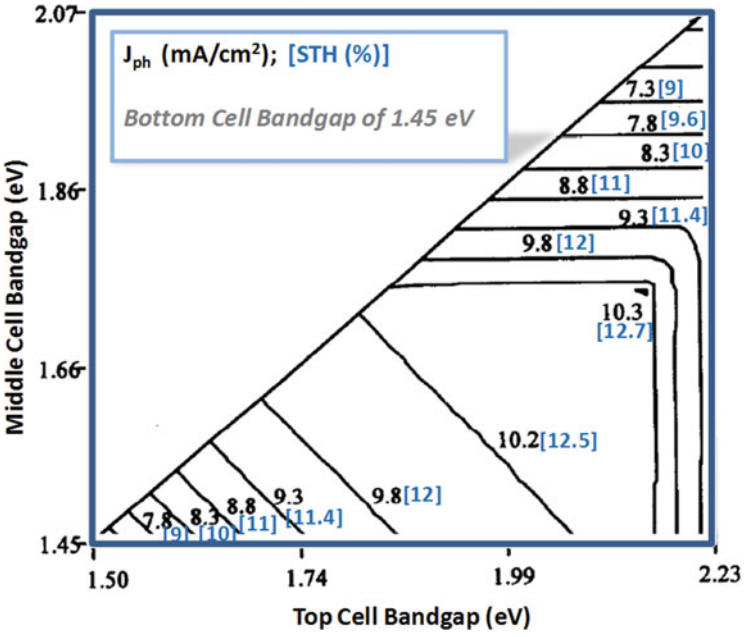

Fig. 7.25 Maximum achievable photocurrent densities and PEC STH efficiencies in triple junction amorphous silicon-based semiconductor devices as a function of top and middle cell bandgaps with a bottom cell gap of 1.45 eV. These results are based on the analyses of Rocheleau and Miller [82] which included solid-state and electrochemical losses

Unfortunately, achieving high STH efficiency levels in laboratory prototypes of thin-film multijunction devices has been elusive to date. Challenges in identifying the most appropriate semiconductor materials to incorporate into a stack, and in developing sufficient solid–solid and solid–liquid interfaces have limited progress. Still, some encouraging research pathways using different device scheme approaches are ongoing.

7.6 PEC Multijunction Device Schemes

A number of different multijunction device schemes incorporating a combination of PEC cells, or a combination of PEC and PV cells have been explored in attempts to enhance solar hydrogen production via water splitting [9, 39, 105]. Some of the device approaches which have demonstrated varying levels of success to date include the following:

1. PV-electrolysis devices with multijunction solid-state PV cells coupled to eletrolyzer systems.
2. Photoelectrode-based PEC–PEC tandem devices incorporating a coupled photoanode and photocathode.
3. Hybrid photoelectrode PV–PEC tandem devices comprising a PEC photoanode or photocathode integrated with a "buried" single-junction PV cell.
4. Hybrid photoelectrode PV–PV–PEC triple-junction devices comprising a PEC photoanode or photocathode integrated with a "buried" double junction PV cell.
5. Photocatalyst Z-scheme systems incorporating hydrogen-evolution and oxygen-evolution photocatalysts in single or dual bed configurations.

In the discussions of these approaches below, schematics of representative device configurations are included, accompanied by the basic device band structures to indicate the energetic driving forces behind the photolytic water splitting. Some examples of implementation in laboratory-scale prototypes are also presented.

7.6.1 Multijunction PV-Electrolysis

Establishing an interesting reference case for multijunction solar water splitting, multijunction PV cells with adequate useable photopotential to directly drive electrolysis have been coupled with electrolyzer systems, which can be separate or fully integrated. This approach is compatible with the "PV-electrolysis" reactor types described in Sect. 7.2.4. However, since the PV output of the multijunction cell is designed to have direct compatibility with electrolysis, no power conditioning units are required. A device level schematic is shown in Fig. 7.26 for the case of a triple-junction PV cell driving the electrolyzer reactions. The useable potential

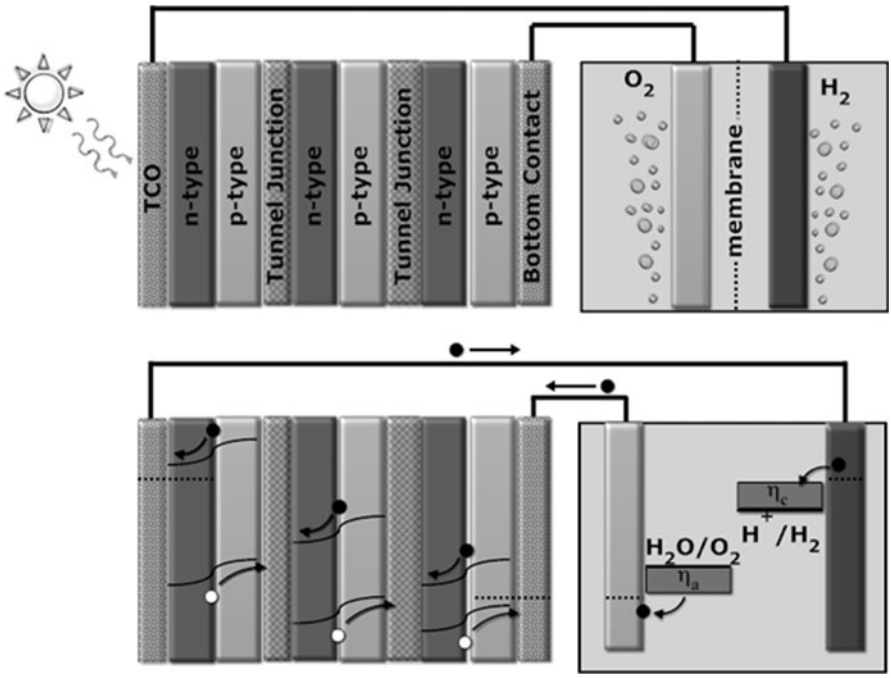

Fig. 7.26 Multijunction PV cell coupled to an electrolyzer system with band diagram showing photogenerated electrons (*black circles*) and holes (*white circles*)

developed by the triple-junction is capable of simultaneously driving photoholes at the electrolyzer anode surface and photoelectrons at the electrolyzer cathode surface. A unique set of design considerations apply in this case. The standard design strategies of current and lattice matching are necessary in the PV semiconductor stack. Additionally, the PV output voltage and current need to be sized to match the optimal operating conditions of the electrolyzer system. The electrolysis process can be independently optimized with appropriate electrodes and catalysts. Since there are no PEC cells in the device stack, any issues of semiconductor durability in solution are avoided. Auxiliary system losses including the lateral collection of current from the PV system and transmission of electrons through external wiring are inevitable, but can be minimized. Also inevitable, cost remains an issue in this approach. As discussed in Sect. 7.2.5, using commercialized PV and electrolyzer technologies, the hydrogen production cost would be greater than $10/kg, far exceeding the US DOE targets of $2–4/kg.

As a potentially lower cost implementation of the PV-electrolysis approach, triple junction amorphous silicon solar cells have been fully integrated with on-board electrolysis units. The amorphous silicon cells generate photovoltages over 2 V, and can convert sunlight to electricity with a stabilize PV efficiency of approximately 8–10%. At the same time, the electrolysis system has been

optimized to convert electricity to hydrogen at efficiencies near 70%. Net STH efficiencies from 5 to 7% are then achievable, as reported by Kelly and Gibson. [106]. The approach is viable, but cost estimates have not been fully developed to evaluate how pragmatic it could be.

Higher efficiency, higher cost multijunction solar cells, such as the III–V materials systems capable of 20–40% PV conversion efficiency are also commercially available. Using these materials, 14–28% STH would be achievable using PV-electrolysis. In today's market, however, such systems would be prohibitively expensive for any large-scale deployment. The 5–7% mark for lower cost amorphous silicon technology is a more appropriate near-term benchmark for practical solar hydrogen production. Alternative PEC-based schemes need to meet or exceed this benchmark to be viable.

7.6.2 PEC–PEC Tandem Photoelectrodes

PEC–PEC tandem photoelectrode systems for solar water splitting have been investigated as one alternative. These comprise separate photoanodes and photocathodes that are optically stacked in series and electrically interconnected, for example, using external wires. The two-photoelectrode approach is compatible with the photoelectrode-based reactor schemes, and subject to the associated reactor-level considerations described in Sect. 7.2.4. A device level schematic of the photoelectrodes is shown in Fig. 7.27, depicting a photoanode stacked in front of a photocathode. The electrode order can be reversed, however, if required by design consideration. For example if a higher bandgap photocathode material is available, this should be the top junction for optical reasons. As seen in the band diagram of Fig. 7.27, the back contacts of two electrodes are directly interconnected, and therefore their electronic levels align. Under illumination, the level of photoelectrons is driven "up" in the photocathode, and the level of photoholes is driven "down" in the photoanode, resulting in sufficient separation to split water.

There are a number of significant design challenges in this approach. The PEC–PEC arrangement requires two different stable PEC semiconductors, one n- and p-type, with added demands of optical compatibility for current matching, and band alignment compatibility for efficient photovoltage generation. As an extra consideration, the front junction must be fabricated on a transparent substrate coated with a transparent conductive layer to enable both light transmission and electron transfer through to the back junction. This adds complication, optical losses, electrical losses, as well as material cost in the photoelectrode fabrication. Additional conductivity losses can be associated with electrode spacing and gas separation. Due to these challenges, efficient PEC/PEC tandem systems have not been demonstrated to date. Proof of concept experiments have been reported, though. For example, a zinc-doped p-type Fe_2O_3 thin film photocathode has been used with a n-type Fe_2O_3 photoanode with reported efficiencies of 0.11%

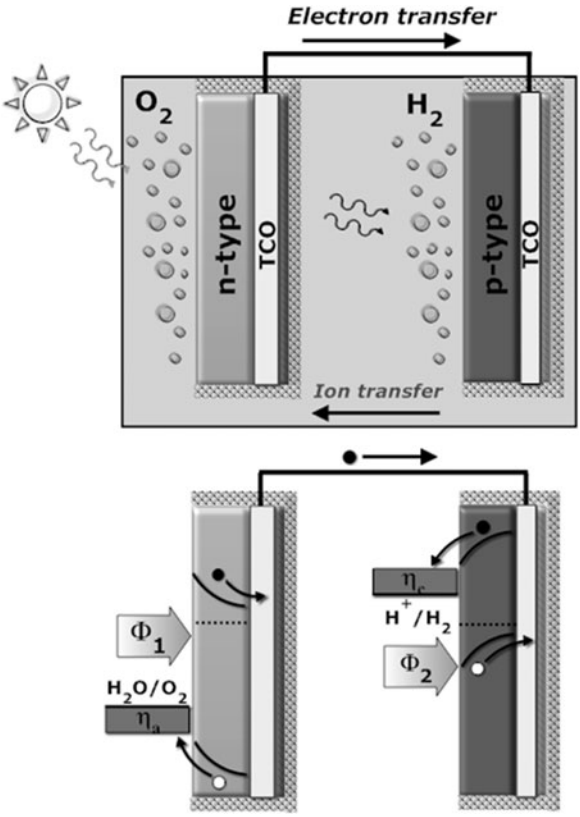

Fig. 7.27 PEC–PEC tandem water splitting device with band diagram showing photogenerated electrons and holes

STH in 0.1 M H_2SO_4 electrolyte [107]. An interesting recent innovation in this area has been the exploration of novel, futuristic tandem nanorod electrode structures using silicon and metal oxides [105].

7.6.3 PV–PEC Tandem Hybrid Photoelectrodes

An alternative tandem device being developed for solar water splitting is the PV/PEC hybrid photoelectrode. In this approach, a PEC top cell is monolithically stacked with a solid-state single-junction PV back cell. Such a photoelectrode device is compatible with both the one- and two-electrode reactor configurations described in Sect. 7.2.4, and the reactor-level considerations described in that section apply. Figure 7.28 shows a device level schematic for a specific two-electrode implementation incorporating a hybrid photocathode and a separate counter electrode. Possible alternative variations include the use of a hybrid photoanode instead of the photocathode, and the integration of the counter and

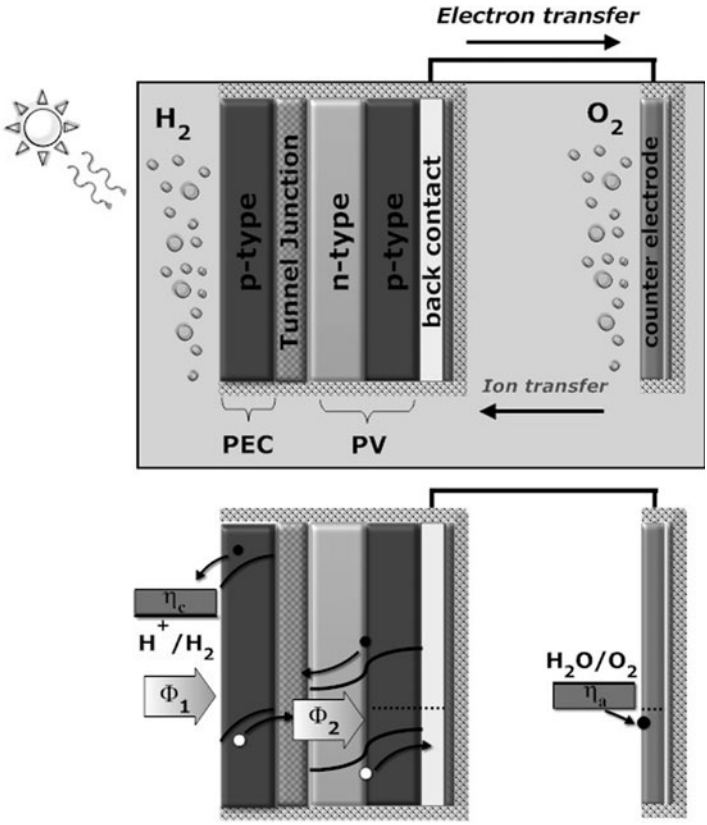

Fig. 7.28 PEC–PV monolithically stacked hybrid water-splitting device

photoelectrodes into a single monolithic device. As seen in the band diagram of Fig. 7.28, the back contact of the PEC cell and the front contact of the PV cell are electronically interconnected via a tunnel junction. In addition, the back contact of the PV cell is wired to the counter electrode, and therefore electronically aligned. As illustrated in the band diagram, under illumination the photoelectron levels at the electrolyte interface and the photohole levels at the counter electrode are separated sufficiently to split water.

In contrast to the PEC–PEC tandem, the two junctions are stacked onto the same substrate, so no transparent substrate is needed. Also, in single-electrode implementations of this approach, electron transmission through wires is eliminated, reducing ohmic losses. There are some clear benefits, but also some specific design challenges associated with the PV–PEC tandem. Appropriately matched PV and PEC semiconductor materials systems are needed, which is challenging enough. In addition, process compatibility in fabricating the PEC cell directly onto the PV cell can be problematic; for example, the necessary restrictions on processing temperature can adversely affect device quality and efficiency. As an alternative strategy for avoiding the process compatibility issues, the PV and PEC cells can be

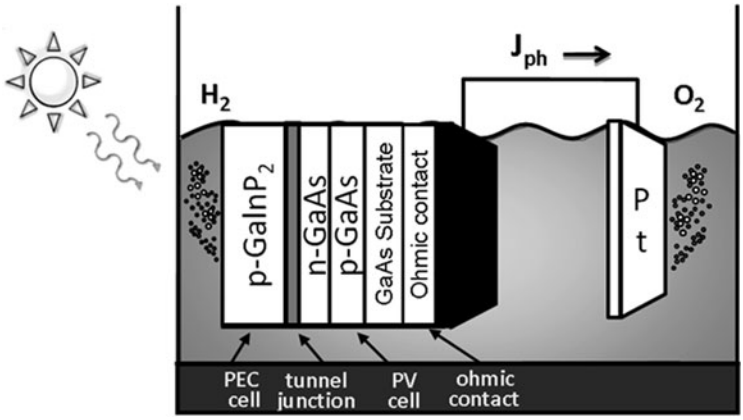

Fig. 7.29 Device schematic of the NREL GaAs/GaInP$_2$ hybrid tandem device submersed in the electrolyte. Light enters through the top GaInP$_2$ PEC electrode then filters down to the GaAs solar cell. This device has demonstrated spontaneous water splitting under illumination with over 12 STH%

separately fabricated and mechanically stacked. This, however, adds manufacturing complexity and new losses. Similar to the tandem PEC–PEC case, stability of the PEC interface is a primary concern in the PV–PEC tandem. There are also similar conductivity losses associated with electrode spacing and gas separation. Overall, it is felt by many that the benefits can outweigh the challenges.

In evidence, the hybrid tandem approach has been under investigation for more than a decade [1, 73, 108, 109]. The best laboratory-scale demonstration to date is unquestionably the NREL's III–V tandem hybrid photoelectrode structure, which still holds the world-record STH efficiency for PEC water-splitting [1, 2]. This hybrid device, shown in Fig. 7.29, consists of a p-type GaInP$_2$ PEC electrode interconnected by a tunnel junction to a buried GaAs p/n PV cell grown on a GaAs wafer substrate. The basic band structure is equivalent to the one shown in Fig. 7.28. In the NREL device, the top junction GaInP$_2$ bandgap is 1.83 eV and the back junction GaAs bandgap is 1.44 eV. Under illumination, hydrogen is evolved at the front photocathode surface and oxygen is evolved at the counter electrode. Under concentrated 11 sun illumination, and in 3 M sulfuric acid electrolyte, prototypes of this device have demonstrated over 12% STH efficiencies for up to 20 h. Subsequent drops in photocurrent and efficiency were reported due to corrosion of the GaInP$_2$. Circumventing the stability limitation, the basic PV structure of this device has also been integrated in tandem-PV-electrolysis prototypes, demonstrating STH efficiencies exceeding 16%. In attempts to enhance the tandem PV–PEC implementation, fundamental research to stabilize the GaInP$_2$ PEC interface is ongoing [97]. Though lacking long-term stability, and reliant on high-cost III–V materials, the results of the NREL demonstrations affirm the potential for high efficiency in multijunction PEC systems. As a "sanity check" for the high-performance levels

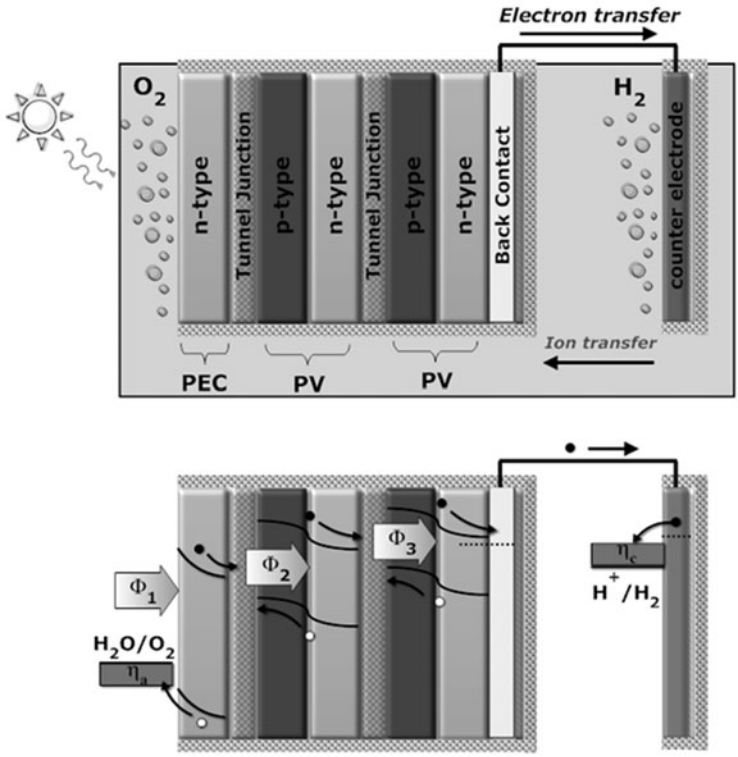

Fig. 7.30 PEC–PV–PV device schematic and band diagram

achieved, it is interesting to note that, according to Fig. 7.23, the STH efficiency limit for a III–V 1.83 eV/1.44 eV tandem stack, is about 18% STH, consistent with the experimental results.

7.6.4 PV–PV–PEC Triple Junction Hybrid Photoelectrodes

A further extension of the PV–PEC hybrid photoelectrode device approach is the PV–PV–PEC triple-junction hybrid photoelectrode. The triple-junction variation is capable of developing higher photopotential, but at the cost of reduced photocurrent and added device complexity. In this configuration, a PEC top cell is monolithically stacked on a solid-state double-junction PV cell. Again, the resulting device is compatible with both the one- and two-photoelectrode configurations in reactor types described in Sect. 7.2.4. A specific two-electrode implementation with a PV–PV–PEC hybrid photoanode and a separate counter electrode is schematically illustrated in Fig. 7.30. Of course, alternative variations include the use of a hybrid

photocathode instead of the photoanode, and the integration of the counter electrode into a single electrode device. Similar to the PV–PEC tandem case, the back contact of the PEC cell and the front contact of the PV–PV double cell are electronically interconnected. Also, the back contact of the PV–PV cell is electronically aligned with the counter electrode. As seen in the band diagram, under illumination the photoelectron levels at the electrolyte interface and the photohole levels at the counter electrode are separated sufficiently to split water. Compared with the PV–PEC tandem, additional photopotential is generated in the PV–PV buried cell of this triple-junction device, offering compatibility with a broader range of lower performing PEC materials. The same design considerations described for the PV–PEC tandem hold, though the extra PV cell adds further complexity and cost in terms of both materials and manufacturing.

The triple-junction hybrid approach has also been well studied, particularly in applications utilizing thin-film metal oxide photoanodes, which frequently require high levels of internal biasing to compensate for unfavorable band positioning at the electrolyte interface. Tungsten trioxide (WO_3), for example, has a proven track record in the stable photo-oxidation of water. However, due to its band structure, biasing in excess of 1.0 V has been needed to achieve water splitting [110]. This has necessitated using a double-junction PV buried cell in triple-junction hybrid photoelectrode applications. At the University of Hawaii (UH) at Manoa, n-type WO_3 thin-film electrodes have been mechanically stacked on top of amorphous silicon (a-Si) tandem PV cells into a PV–PV–PEC hybrid device, as illustrated in Fig. 7.31a [7]. The "load-line" analysis of this device [54] is shown in Fig. 7.31b, superimposing the independently measured two-electrode response curves of both the WO_3 PEC (in 0.33 M H_3PO_4) cell and the a-Si tandem PV cell under AM1.5G illumination [57]. Consistent with the operating point indicated by the intersection in the load-line plot, the device successfully split water, with a stabilized photocurrent of 2.5 mA/cm^2, corresponding to a STH conversion efficiency of approximately 3.1%. An interesting and important insight from the load-line plot is that the limiting factors to high efficiency in this specific device are the WO_3 onset potential, saturation photocurrent, and fill factor. If these could be adequately addressed, such a triple-junction approach using low cost thin film semiconductor materials has clear potential for exceeding 5% STH. Based on the optical limits, as seen in Fig. 7.25, successful bandgap reduction in the WO_3 would be needed to exceed the 5% mark. Alternatively, new lower bandgap thin-film materials may emerge through research for this application.

In addition to the amorphous silicon implementation, several interesting variations of the PV–PV–PEC hybrid device based on WO_3 photo-oxidation cells have been demonstrated focusing on low-cost material components. Most notably is the impressive work using tungsten oxide PEC cells in conjunction with dye-sensitized solar cells. The Grätzel–Augustynski "Tandem Cell" is the best example of this [5], though some more recent work has been reported by the Arakawa group in Japan [111]. Efficiencies in these all-PEC configurations are reported in the 2.5–4.5% STH range. Moreover, there has been commercial interest in this approach.

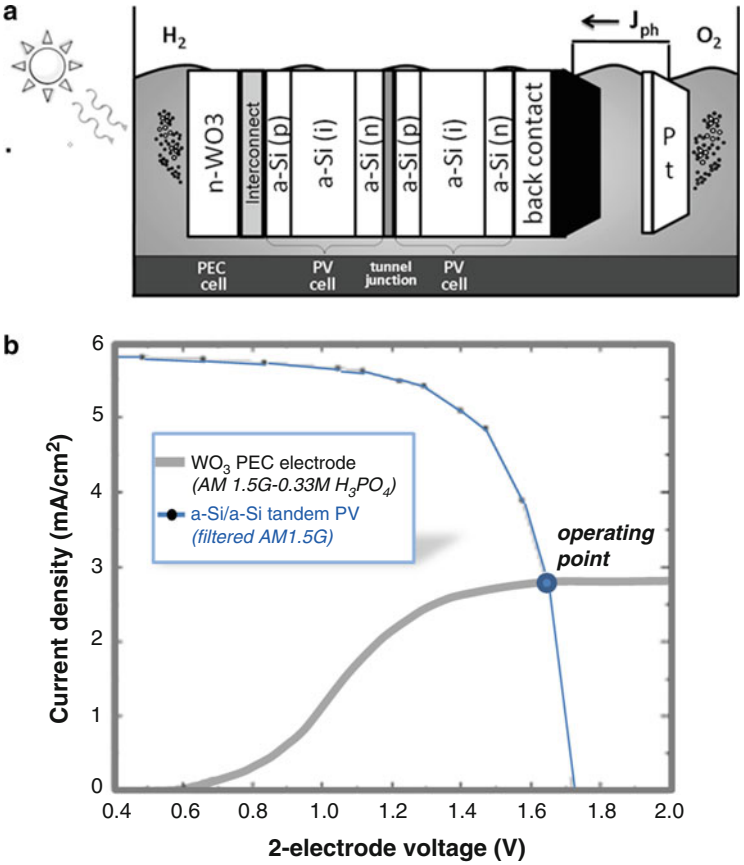

Fig. 7.31 (**a**) Device schematic of the UH WO_3/a-Si/a-Si hybrid triple junction device submerged in the electrolyte. Light enters through the top WO_3 PEC electrode then filters down to a-Si/a-Si tandem solar cell. This device has demonstrated spontaneous water splitting under illumination with over 3.0 STH%. (**b**) Load-line analysis of the device, showing operating point of 2.5 mA/cm^2 based on superposition of the PV and PEC responses

Another interesting example has been the development of an all thin-film silicon triple-junction hybrid device by MVSystems, Incorporated [109, 112–114]. In this device, hydrogenated amorphous silicon-carbide alloy thin-films are used for all three junctions, including the PEC junction and both buried PV cells. Bandgap tuning through alloy composition variations is used for current matching. Compatible with the triple-junction efficiency analysis shown in Fig. 7.25, such a device has theoretical potential for exceeding 10% STH. Laboratory prototypes, though, have been limited by high-loss potential barriers formed at the PEC interface, and demonstrations to date of spontaneous solar water splitting have performed closer to 1% STH. Ongoing work to reduce the interfacial barrier issues offers much promise for achieving commercialized PEC hydrogen production based on thin-film silicon alloys.

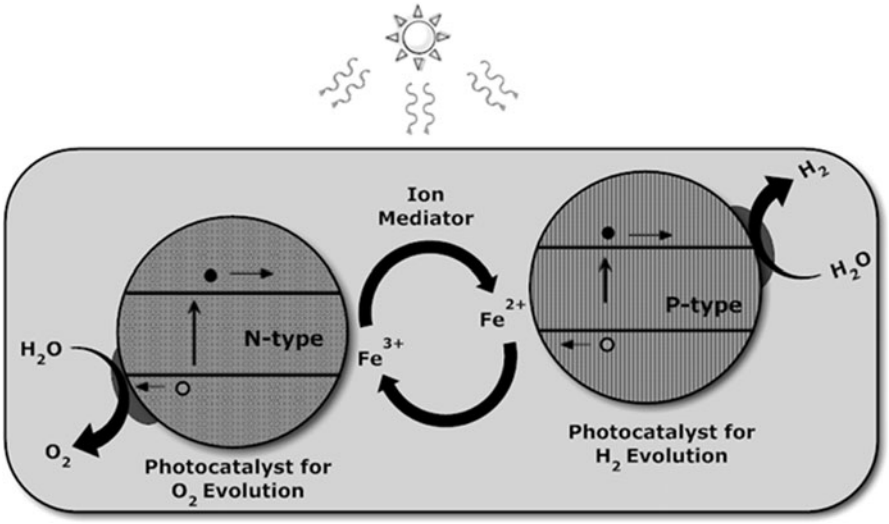

Fig. 7.32 Energy band diagram of the Z-scheme showing OER and HER photocatalyst particles with functionalized surface sites for the oxygen- and hydrogen-evolution reactions, respectively. Concentrations of both particle types are suspended together in solution with an ion-shuttling mediator, such as the Fe^{3+}/Fe^{2+} couple, effectively coupling the gas evolution reactions in tandem to photosplit water

7.6.5 Photocatalyst Z-Schemes

The "Z-scheme" approach, which is receiving much recent attention, particularly in the Japanese research community, is essentially a photocatalyst version of the tandem PEC–PEC photoelectrode system. As shown in the schematic representation in Fig. 7.32, n-type photocatalyst particles drive the hydrogen evolution reaction (HER) and p-type photocatalyst particles drive the oxygen evolution reaction (OER), achieving water splitting in a tandem fashion. In the Z-scheme, electrons are exchanged between the photoanode and photocathode particles via an ion mediator in solution (such as the Fe^{3+}/Fe^{2+} couple), rather than through wires, as in the PEC–PEC photoelectrode case. Slurries of the two photocatalysts can be mixed together in single-bed reactors, or alternatively, slurries of the HER and OER photocatalysts can be separated into two beds, connected with an ionic bridge, consistent with the one- and two-bed reactors discussed in Sect. 7.2.4.

As indicated in the DTI techno-economic analysis report, the particle-based systems offer some of the best hope for low-cost hydrogen production on a large scale, but there are a number of unique design challenges posed by this approach. For example, charge separation within each catalyst particle needs to be enhanced. The photocathode particle has to simultaneously reduce hydrogen and oxidize the mediator at separate surface sites. Similarly, the photoanode particle must both

oxidize water and reduce the mediator. Functionalization of surface sites, for example, with reaction-specific nanoparticle catalysts, is necessary to draw apart photogenerated electrons and holes, and to enable the simultaneous reactions.

As a particular challenge in the single bed reactor system using Z-scheme photocatalysts, both hydrogen and oxygen are evolved in the same reactor bed, with associated safety hazards. Safe gas separations techniques could be employed, but at substantial additional cost. The dual bed system avoids any possible explosive hydrogen/oxygen gas mixtures, but the greater land area requirements and conductivity losses in the ion bridge reduce the STH performance. Both the single- and dual-bed systems have their advantages and disadvantages, but either way, new HER and OER photocatalysts need to be identified with sufficient efficiency and stability for practical hydrogen production.

The search for effective HER and OER photocatalyst materials for Z-scheme systems is ongoing. Extensive libraries of multicomponent metal oxides and oxinitrides are being developed and screened [9, 96–99]. Specific material systems have demonstrated spontaneous water-splitting under visible light, for example, $SrTiO_3$:Rh combined with $BiVO_4$ in the presence of an Fe^{3+}/Fe^{2+} redox couple [115], but STH efficiencies remain extremely low. Visible light water splitting has also been accomplished using a RuO_2–TaON and Pt–TaON mixture with I_3^-/I^- redox couple, but again with low STH efficiency [116]. A recurring theme in PEC research is that new materials continue to offer new hope.

7.6.6 Many Options

Compared with the photovoltaics industry, the field of multijunction PEC hydrogen production is relatively new, but there has been substantial exploratory research in recent years. In addition to the above examples in *PV-electrolysis, multijunction photoelectrolysis*, and *Z-scheme photocatalysis*, numerous variations which mix and match concepts and components of all three are conceivable. In the final analysis, commercialization will depend on balances between performance, complexity, and cost. The simpler the system, the better. Single-junction photocatalyst or photoelectrode systems offer the greatest simplicity, but the significant difficulties in achieving high efficiencies in these systems necessitate a serious look at the multijunction alternatives. Efficient tandem systems are the next best hope. Analysis has validated the potential for high STH conversion efficiencies in tandem double- and triple-junction schemes and there has been experimental verification, though still limited, on the laboratory scale. Real challenges remain in the identification of low-cost material systems capable of reproducing the laboratory performance levels on a commercial scale. As the research community advances in its ability to engineer high-efficiency absorber materials and functionalized interfaces, and as it learns to integrate these in optimal multijunction designs, the opportunities for success will continue to grow.

7.7 In Summary

There have been significant R&D efforts over the past several decades advancing multijunction device technologies, particularly in the PV field. These have resulted in the highest solar-to-electric conversion efficiencies to date, exceeding 40% in high quality III–V cells being commercialized for space applications. These ultrahighly efficient cells are, however, expensive, and not practical for large-scale deployment in solar power production plants. The multijunction approach continues to make strides in improving performance in lower cost thin-film solar cells, including, for example, amorphous silicon and copper chalcopyrite devices, though the commercial benefits have not yet been fully realized. It is nevertheless clear that low cost and high performance are the keys to the success of transformative scale solar electricity. Multijunction thin film devices offer hope in this area, and this hope extends to PEC hydrogen production.

There are more recent efforts to develop multijunction devices and systems for solar hydrogen production, though this field is still in its infancy in comparison with PV technologies. STH conversion efficiencies of 12–16% have been demonstrated on the laboratory scale in tandem devices using high-quality III–V materials, but with limited durability. Multijunction PEC and PV-electrolysis systems using lower cost thin-film materials have demonstrated better stability, but at conversion efficiencies limited in the 3–8% range. Ultimately, durable, low cost systems with STH conversion efficiencies over 10% are needed for commercial deployment of solar hydrogen technologies. Fortunately, continued development of multijunction schemes offers great promise, specifically in terms of enhanced photopotentials and broadened spectral bandwidth. Analyses of tandem and triple-junction PEC schemes indicate that efficiencies exceeding 10% STH and in special cases up to 25% STH, are in fact possible. Technical barriers have stood in the way of achieving such performance levels, but these are solvable if the fundamental problems are broken down and appropriately addressed.

7.7.1 What Is Needed?

Based on PEC research efforts to date, it has become increasingly clear that new, innovative material systems, interfaces, and devices are needed to achieve high-performance, low-cost solar water splitting. Breaking this down into specifics relative to the multijunction approach:

- Low-cost semiconductor materials with appropriate bandgap and sufficient opto-electronic quality need to be identified and optimized to enable efficient solar energy absorption and charge extraction.
- Effective PEC interfaces activated for the gas evolution reactions and passivated for corrosion and other parasitic reactions need to be engineered, using, for example, heterojunction and/or catalytic coating and/or dispersions.

- Low loss solid-state interfaces need to be engineered for bridging component cells in a multijunction device structure, for example, using tunnel junctions or intermediate transparent conductive oxides layers.
- Innovative multijunction designs combining the best materials and interfacing schemes into efficient photoelectrode or photocatalyst device structures will be the key.
- Innovative synthesis and fabrication techniques will be needed to enable cost-effective large-scale manufacture of multijunction photoelectrodes or photocatalysts.

Leveraging the knowledge gained from the PV community in the successful development of high-efficiency multijunction device designs will be integral to success. Key advances, however, are needed specifically in the development of the PEC material components and interfaces, since these remain the greatest technical barriers.

7.7.2 What Is Happening

In efforts to address the technical barriers, the PEC research community over the past several years has been developing new theoretical, synthesis and characterization tools using improved state-of-the-art methodologies [57]. These tools are being employed in several parallel strategies for developing the innovative materials and interfaces necessary to the success of PEC hydrogen production systems.

One specific approach is the further development of the traditional PEC semiconductor materials in thin-film and nanostructured forms for higher efficiencies. There have been significant scientific efforts in this approach, including continued development of the following materials classes:

- Tungsten-oxide and related bandgap-reduced compounds [6, 117–121].
- Iron-oxide and related enhanced mobility compounds [122–126].
- Vanadates, including bismuth vanadate and related compounds [127–129].
- Titanium dioxide and related bandgap-reduced compounds [61, 130].

This list is by no means comprehensive, but does represent a large part of the research endeavors to advance well-established PEC semiconductors.

Another important strategy is the adaptation of efficient PV semiconductor thin-films and nanostructures for effective use in PEC applications. Recent research in this area has focused on material classes with inherent bandgap tuning capabilities such as the amorphous silicon compounds (including silicon carbides and nitrides) [109, 112–114, 131, 132], and polycrystalline copper chalcopyrite compounds [133–137].

Some of the most recent innovative approaches have included the development of entirely new materials classes and structures for use in photoelectrode or photocatalyst devices. Examples include quantum-confined WS_2 and MoS_2

nanoparticle photocatalysts embedded in a conductive scaffolding [138] and silicon nanorods embedded in membrane structures [105, 139]. Also cutting-edge are efforts in the development of breakthrough synthesis technologies to reduce the cost and enhance the stability of the high-performance III–V multijunction structures that have demonstrated the best efficiencies to date, both in PV and PEC [4, 87]. Future progress in all these approaches, which will be integral to the ultimate success of PEC hydrogen production, will depend on the best use of the most advanced research tools.

7.7.3 The Path Forward

For all PEC systems, and for multijunction water-splitting systems in particular, the fundamental solutions reside in *MATERIALS* and *INTERFACES*. Good solid-state light absorber materials with efficient charge transport properties that can be synthesized inexpensively are the cornerstone. Low loss interfaces are the next major step. For example, low-defect and low-recombination solid-state interfaces are essential between cells in a multijunction stack, and at back contacts. These are achievable, as demonstrated through years of R&D in the PV research community. More challenging are the solid–liquid electrochemical interfaces in PEC multijunction schemes. Functionalizing surfaces to produce the right energetic and kinetics for promoting the water-splitting half reactions while inhibiting parasitic reactions and recombination loss will be the key to unlock the full potential of PEC hydrogen production.

The lessons learned to date in the PEC research and development community, coupled with of PV knowledge and experience amassed over decades could be extremely fruitful, both for solar hydrogen and solar electricity production. Some questions to consider for the pathways forward include the following:

- Can functions of light absorption, charge extraction, reaction catalysis, and production management be effectively separated, and independently optimized in PEC devices? If so, it opens up the design space considerably. For example, a good absorber material would not need to be catalytic, but could be coupled with a good catalyst material with the design of an efficient interface.
- Can cost-effective thin film PV materials (e.g., amorphous silicon or more efficient copper chalcopyrites) and multijunction devices be adapted through surface modifications to split water? If so, a wealth of PV manufacturing experience would be available for enabling commercial scale deployment.
- Can new low-cost synthesis routes be devised for ultrahigh efficiency III–V materials and devices? If so, the barriers to large-scale deployment of solar electricity are largely gone. Moreover, if appropriate surface modifying materials and interfaces are also developed, then the commercial viability of PEC hydrogen production would be assured.

- Can new forms of earth-abundant materials, including oxides, nitrides, and sulfides, be discovered and developed with sufficiently good light absorbing and charge transport properties for solar energy conversion? This, with the development of efficient solid-state and electrochemical interfaces, and with the design of effective multijunction photoelectrode or photocatalyst systems, could revolutionize both PV and PEC technologies!

These questions encompass a broad vision and provide a coarse roadmap for paths forward. The pathways to success of PEC hydrogen production are along the road of technical collaboration; and the trail will be blazed by the new generation of scientists and engineers.

Acknowledgments The authors would like to acknowledge and express their great admiration for all members of the international PEC research and development community; with special nods of appreciation to the US Department of Energy's PEC Working Group supported by the Fuel Cells Technologies Office, and to Annex-26 of the International Energy Agency's Hydrogen Implementing Agreement. They also thank the members of the Thin Films Laboratory at the University of Hawaii at Manoa's Hawaii Natural Energy Institute, including Drs. Nicolas Gaillard, Bor Yann Liaw, Yuancheng Chang, and Richard Rocheleau, as well as Jess Kaneshiro, Jeremy Kowalczyk, Xi Song, and Brett Ikei for their encouragement and support to this effort.

References

1. Khaselev, O., Bansal, A., Turner, J.A.: High-efficiency integrated multijunction photovoltaic/electrolysis systems for hydrogen production. Int. J. Hydrogen Energy **26**, 127–132 (2001)
2. Khaselev, O., Turner, J.A.: A monolithic photovoltaic photoelectrochemical device for hydrogen production via water splitting. Science **280**, 425–427 (1998)
3. Andreev, V.M.: GaAs and high-efficiency space cells. In: Markvart, T., Castañer, L. (eds.) Practical Handbook of Photovoltaics: Fundamentals and Applications. Elsevier, New York (2003)
4. Deutsch, T.G., Koval, C.A., Turner, J.A.: III − V nitride epilayers for photoelectrochemical water splitting: GaPN and GaAsPN. J. Phys. Chem. B **110**, 25297–25307 (2006)
5. Grätzel, M.: Photoelectrochemical cells. Nature **414**, 338 (2001)
6. Marsen, B., Miller, E.L., Paluselli, D., Rocheleau, R.E.: Progress in sputtered tungsten trioxide for photoelectrode applications. Int. J. Hydrogen Energy **32**, 3110–3115 (2007)
7. Gaillard, N., Chang, Y., Kaneshiro, J., Deangelis, A., Miller, E.L.: Status of research on tungsten oxide-based photoelectrochemical devices at the University of Hawai'i. Proc. SPIE **7770**, 77700V–77701V (2010)
8. Rocheleau, R.E., Miller, E.L., Misra, A.: High-efficiency photoelectrochemical hydrogen production using multijunction amorphous silicon photoelectrodes. Energy Fuels **12**, 3–10 (1998)
9. Miller, E.L., Gaillard, N., Kaneshiro, J., DeAngelis, A., Garland, R.: Progress in new semiconductor materials classes for solar photoelectrolysis. Int. J. Energy Res **34**, 1215–1222 (2010)
10. Kuang, C.: Fast Company. http://www.fastcompany.com/blog/cliff-kuang/design-innovation/start-aims-clean-energys-holy-grail-freeing-hyrodgen-water, 16 Apr 2009. Accessed 29 Mar 2011
11. Li, Y., Zhang, J.Z.: Hydrogen generation from photoelectrochemical water splitting based on nanomaterials. Laser Photonics Rev. **4**, 517–528 (2010)

12. Bush, G.W.: State of the Union. Presented in Washington, DC, USA, 28 January 2003
13. Rifkin, J.: The Hydrogen Economy. Tarcher (2003)
14. Romm, J.J.: The Hype About Hydrogen. Island, New York (2004)
15. Bromaghim, G., Gibeault, K., Serfass, J., Serfass, P., Wagner, E.: Hydrogen and Fuel Cells: The U.S. Market Report. National Hydrogen Association, 22 March 2010
16. Collodi, G., Bressan, L., Ruggeri, F., Uncuoglu, D.: Hydrogen Production for Upgrading Projects in Refineries. Foster Wheeler Italiana S.p.A, Via Caboto 1, 20094 Corsico – Milan – Italy. http://www.fwc.com/publications/tech_papers/files/Hydrogen%20Production%20for%20Upgrading%20in%20Refineries.pdf (2009). Accessed 29 Mar 2011
17. U.S. Department of Energy: Natural Gas Reforming. http://www1.eere.energy.gov/hydrogenandfuelcells/production/natural_gas.html. Accessed 29 Mar 2011
18. Ball, M., Wietschel, M.: The Hydrogen Economy: Opportunities and Challenges. Cambridge Press, New York (2009)
19. Yürüm, Y.: Hydrogen energy system: production and utilization of hydrogen and future aspects. Kluwer Academic Publishers, Dordrecht (1995)
20. Turner, J.A.: A realizable renewable energy future. Science **285**, 687–689 (1999)
21. Energy Information Administration: World Proved Reserves of Oil and Natural Gas, Most Recent Estimates. 3 March 2009. http://www.eia.doe.gov/emeu/international/reserves.html. Accessed 29 Mar 2011
22. Energy Information Administration: World Petroleum Consumption, 1960–2008. http://www.eia.doe.gov/aer/txt/ptb1110.html. Accessed 29 Mar 2011
23. Energy Information Administration: International Energy Outlook 2007: Petroleum and Other Liquid Fuels. http://www.eia.doe.gov/oiaf/archive/ieo07/pdf/oil.pdf. Accessed 29 Mar 2011
24. Safina, C.: Testimony to the House Subcommittee on Energy and Environment. 21 May 2010
25. U. S. Department of Energy, Office of Science: Basic Research Needs for Solar Energy Utilization. Washington (2005)
26. Green, M.A.: Solar cells: Operating Principles, Technology, and System Applications. Prentice-Hall, Inc, Kensington, NSW (1982)
27. U. S. Department of Energy, Energy Information Administration: International Energy Outlook 2008 (DOE/EIA-0484). Washington (2008)
28. Greentech Media and the Prometheus Institute: PV Technology, Production and Cost, 2009 Forecast: The Anatomy of a Shakeout. Cambridge (2008)
29. Solarbuzz: Marketbuzz 2009: Annual World Solar PV Market Report. San Francisco (2009)
30. Bauman, R.P.: Modern Thermodynamics with Statistical Mechanics. Macmillan Publishing Company, New York (2003)
31. Akkerman, I., Janssen, M., Rocha, J., Wijffels, R.H.: Photobiological hydrogen production: photochemical efficiency and bioreactor design. Int. J. Hydrogen Energy **27**, 1195–1208 (2002)
32. Zaborsky, O.R.: Biohydrogen. Plenum, New York (1998)
33. Funk, J.E., Reinstrom, R.M.: Energy requirements in production of hydrogen from water. Ind. Eng. Chem. Process Des. Dev. **5**, 336–342 (1966)
34. Minggu, L.J., Daud, W.R.W., Kassim, M.B.: An overview of photocells and photoreactors for photoelectrochemical water splitting. Int. J. Hydrogen Energy **35**, 5233–5244 (2010)
35. James, B.D., Baum, G.N., Perez, J., Baum, K.N.: Technoeconomic Analysis of Photoelectrochemical (PEC) Hydrogen Production. Directed Technologies, Inc. https://www1.eere.energy.gov/hydrogenandfuelcells/pdfs/pec_technoeconomic_analysis.pdf (2009). Accessed 11 Mar 2011
36. Ruth, M., Laffen, M., and Timbario, T.A.: NREL technical report (NREL/BK-6A1-46676). Hydrogen Pathways: Cost, Well-to-Wheels Energy Use, and Emissions for the Current Technology Status of Seven Hydrogen Production, Delivery, and Distribution Scenarios. September 2009

37. NREL Technical Report (NREL/TP-6A1-46612): Current (2009) State-of-the-Art Hydrogen Production Cost Estimate Using Water Electrolysis. September 2009
38. DOE EERE Fuel Cells Technologies Program: Multi-Year Research, Development and Demonstration Plan: Planned Program Activities for 2005–2015. http://www1.eereenergy.gov/hydrogenandfuelcells/mypp/. April 2009
39. Kelly, N.A., Gibson, T.L.: Solar energy concentrating reactors for hydrogen production by photoelectrochemical water splitting. Int. J. Hydrogen Energy **33**, 6420–6643 (2008)
40. Mavroides, J.G., Kafalas, J.A., Kolesar, D.F.: Photoelectrolysis of water in cells with $SrTiO_3$ anodes. Appl. Phys. Lett. **28**, 241–243 (1976)
41. Bard, A.J., Faulknerk, L.R.: Electrochemical Methods: Fundamentals and Applications. Wiley, New York (2000)
42. Bockris, J.O.M., Reddy, A.K.N., Gamboa-Aldeco, M.E.: Modern Electrochemistry: Fundamentals of Electrodics, vol. 2a. Springer, New York (2001)
43. Memming, R.: Semiconductor Electrochemistry. Wiley-VCH, Weinheim (2001)
44. Lipkowski, J., Ross, P.N.: Electrochemistry of Novel Materials. VCH Publishers, New York (1994)
45. Gellings, P.J., Bouwmeester, H.J.M.: The CRC Handbook of Solid State Electrochemistry. CRC, Boca Raton (1997)
46. Nozik, A.J., Memming, R.: Physical chemistry of the semiconductor–liquid interface. J. Phys. Chem. **100**, 13061–13078 (1996)
47. Gerischer, H.: Solar photoelectrolysis with semiconductor electrodes. In: Seraphin, B.O. (ed.) Solar Energy Conversion, Solid-State Physics Aspects, pp. 115–172. Springer-Verlag, New York (1979)
48. Gerischer, H.: Physical Chemistry: An Advanced Treatise, vol. 9A. Academic, New York (1970)
49. Gerischer, H.: The impact of semiconductors on the concept of electrochemistry. Electrochim. Acta **35**, 1677–1690 (1990)
50. Miller, E.L.: Solar hydrogen production by photoelectrochemical water splitting: the promise and challenge. In: Vayssieres, L. (ed.) On Solar Hydrogen and Nanotechnology, pp. 3–35. Wiley, Asia (2009)
51. Lee, K., Nam, W.S., Han, G.Y.: Photocatalytic water-splitting in alkaline solution using redox mediator. 1: Parameter study. Int. J. Hydrogen Energy **29**, 1343–1347 (2004)
52. Marcus, R.J.: Chemical conversion of solar energy. Science **123**, 399–405 (1965)
53. Bockris, J.O.M.: Kinetics of activation controlled consecutive electrochemical reactions: anodic evolution of oxygen. J. Chem. Phys. **24**, 817–827 (1956)
54. Kanan, M.W., Nocera, D.G.: In Situ Formation of an oxygen-evolving catalyst in neutral water containing phosphate and Co^{2+}. Science **321**, 1072–1075 (2008)
55. Dutta, S.: Technology assessment of advanced electrolytic hydrogen production. Int. J. Hydrogen Energy **15**, 379–386 (1990)
56. LeRoy, R.L.: Industrial water electrolysis: present and future. Int. J. Hydrogen Energy **8**, 401–417 (1983)
57. Chen, Z., Jaramillo, T.F., Deutsch, T.G., Kleiman-Shwarsctein, A., Forman, A.J., Gaillard, N., Garland, R., Takanabe, K., Heske, C., Sunkara, M., McFarland, E.W., Domen, K., Miller, E.L., Turner, J.A., Dinh, H.N.: Accelerating materials development for photoelectrochemical (PEC) hydrogen production: Standards for methods, definitions, and reporting protocols. J. Mater. Res. **25**, 3–16 (2010)
58. Parkinson, B.: On the efficiency and stability of photoelectrochemical devices. Acc. Chem. Res. **17**, 431–437 (1984)
59. Dohrmann, J.K., Schaaf, N.S.: Energy conversion by photoelectrolysis of water: determination of efficiency by in situ photocalorimetry. J. Phys. Chem. **96**, 4558–4563 (1992)
60. Heller, A.: Electrochemical solar cells. Solar Energy **29**, 153–162 (1982)
61. Khan, S.U.M., Al-shahry, M., Ingler Jr., W.B.: Efficient photochemical water splitting by a chemically modified n-TiO_2. Science **297**, 2243–2245 (2002)

62. Emery, K.: Measurements and characterization of solar cell modules. In: Luque, A., Hegedus, S. (eds.) Handbook of Photovoltaic Science and Engineering, pp. 701–752. Wiley, New York (2003)
63. NIST Chemistry WebBook: NIST Standard Reference Database Number 69 http://webbook.nist.gov/chemistry/. Accessed 29 Mar 2011
64. Luther, J.: Motivation for photovoltaic application and development. In: Luque, A., Hegedus, S. (eds.) Handbook of Photovoltaic Science and Engineering, pp. 45–60. Wiley, New York (2003)
65. Asahi, R., Morikawa, T., Ohwaki, T., Aoki, K., Tage, Y.: Visible-light photocatalysis in nitrogen-doped titanium oxides. Science **293**, 269 (2001)
66. Sze, S.M.: Physics of Semiconductor Devices. Wiley, New York (2006)
67. Neamen, D.A.: Semiconductor Physics and Devices: Basic Principles. McGraw-Hill, New York (2002)
68. Balandin, A.A., Wang, K.L.: Handbook of Semiconductor Nanostructures and Nanodevices (5-Volume Set). American Scientific Publishers, Stevenson Ranch (2006)
69. Muller, R.S., Kamins, T.I.: Device Electronics for Integrated Circuits. Wiley, New York (2002)
70. Yu, P.Y., Cardona, M.: Fundamentals of Semiconductors: Physics and Materials Properties. Springer, New York (2004)
71. Mussini, T., Longhi, P.: Chlorine. In: Bard, A.J., Parsons, R., Jordan, J. (eds.) Standard Potentials in Aqueous Solution, pp. 70–77. IUPAC, New York (1985)
72. Tan, M.X., Kenyon, C.N., Krulger, O., Lewis, N.S.: Behavior of Si photoelectrodes under high level injection conditions. 1. Steady-state current–voltage properties and quasi-fermi level positions under illumination. J. Phys. Chem. B **101**, 2830–2839 (1997)
73. Miller, E.L., Paluselli, D., Marsen, B., Rocheleau, R.: Optimization of hybrid photoelectrodes for solar water splitting. Electrochem. Solid-State Lett. **8**, A247–A249 (2005)
74. Hanna, M.C., Nozik, A.J.: Solar conversion efficiency of photovoltaic and photoelectrolysis cells with carrier multiplication absorbers. J. App. Phys. **100**, 074510 (2006)
75. Ross, R.T., Hsiao, T.L.: Limits on the yield of photochemical solar energy conversion. J. Appl. Phys. **48**, 4783–4785 (1977)
76. Bolton, J.R., Haught, A.F., Ross, R.T.: Photochemical energy storage: an analysis of limits. In: Connolly, J.S. (ed.) Photochemical Conversion and Storage of Solar Energy, pp. 297–330. Academic, New York (1981)
77. Bolton, J.R., Strickler, S.J., Connolly, J.S.: Limiting and realizable efficiencies of solar photolysis of water. Nature **316**, 495–500 (1985)
78. Weber, M.F., Dignam, M.J.: Splitting water with semiconducting photoelectrodes – efficiency considerations. Int. J. Hydrogen Energy **11**, 225 (1986)
79. Archer, M.D., Bolton, J.R.: Requirements for ideal performance of photochemical and photovoltaic solar energy converters. J. Phys. Chem. **94**, 8028–8036 (1990)
80. Bolton, J.R.: Solar photoproduction of hydrogen: a review. Solar Energy **57**, 37 (1996)
81. Licht, S.: Multiple band gap semiconductor/electrolyte solar energy conversion. Phys. Chem. B **105**, 6281–6294 (2001)
82. Rocheleau, R.E., Miller, E.L.: Photoelectrochemical production of hydrogen: engineering loss analysis. Int. J. Hydrogen Energy **22**, 771–782 (1997)
83. Ellis, A.B., Kaiser, S.W., Wrighton, M.S.: Semiconducting potassium tantalate electrodes. J. Phys. Chem. **80**, 1325–1328 (1976)
84. Green, M.A.: Third Generation Photovoltaics: Advanced Solar Energy Conversion. Springer-Verlag, Heidelberg (2003)
85. Yamaguchi, M.: Super-high-efficiency multi-junction solar cells. Prog. Photovolt. Res. Appl. **13**, 125 (2005)
86. King, R.R. et al: Advances in High-Efficiency III-V Multijunction Solar Cells. Adv. Opto-Electr. Article ID 29523, 8 pages (2007)

87. Press Release: Spectrolab solar cell breaks 40% efficiency barrier. 7 December 2006. http://www.insidegreentech.com/node/454. Accessed 29 Mar 2011
88. Guter, W., et al.: Current-matched triple-junction solar cell reaching 41.1% conversion efficiency under concentrated sunlight. Appl. Phys. Lett. **94**, 223504 (2009)
89. Swinehart, D.F.: The Beer–Lambert law. J. Chem. Educ. **39**, 333 (1962)
90. López, N., Reichertz, L.A., Yu, K.M., Campman, K., Walukiewicz, W.: Engineering the electronic band structure for multiband solar cells. Phys. Rev. Lett. **106**, 028701 (2011)
91. Baruch, P., De Vos, A., Landsberg, P.T., Parrott, J.E.: On some thermodynamic aspects of photovoltaic solar energy conversion. Solar Energy Mater. Solar Cells **36**, 201–222 (1995)
92. Fonash, S.: Solar Cell Device Physics. Academic, New York (1982)
93. Smestad, G.P.: Optoelectronics of Solar Cells. SPIE, Bellingham (2002)
94. Yang, J., Yan, B., Guha, S.: Amorphous and nanocrystalline silicon-based multi-junction solar cells. Thin Solid Films **487**, 162–169 (2005)
95. Nishiwaki, S., Siebentritt, S., Walk, P., Lux-Steiner, M.C.: A stacked chalcopyrite thin-film tandem solar cell with 1.2 V open-circuit voltage. Prog. Photovolt. Res. Appl. **11**, 243–248 (2003)
96. Arai, T., Konishi, Y., Iwasaki, Y., Sugihara, H., Sayama, K.: High-throughput screening using porous photoelectrode for the development of visible-light-responsive semiconductors. J. Comb. Chem. **9**, 574–581 (2007)
97. Kusama, H., Wang, N., Miseki, Y., Sayama, K.: Combinatorial search for iron/titanium-based ternary oxides with a visible-light response. J. Comb. Chem. **12**, 356–362 (2010)
98. Jianghua, H., Parkinson, B.A.: A combinatorial investigation of the effects of the incorporation of Ti, Si, and Al on the performance of α-Fe_2O_3 photoanodes. J. Comb. Chem. **13**(4), 399–404 (2011)
99. Woodhouse, M., Parkinson, B.A.: Combinatorial approaches for the identification and optimization of oxide semiconductors for efficient solar photoelectrolysis. Chem. Soc. Rev. **38**, 197–210 (2009)
100. Burnett, B.: The Basic Physics and Design of III-V Multijunction Solar Cells. NREL, Golden (2002)
101. Yamaguchi, M.: III–V compound multi-junction solar cells: present and future. Solar Energy Mater. Solar Cells **75**, 261–269 (2003)
102. Wolf, M.: Limitations and possibilities for improvement of photovoltaic solar energy converters. Proc. Inst. Radio Eng. **48**, 1246–1263 (1960)
103. Poortmans, J., Arkhipov, V.: Thin film solar cells: fabrication, characterization and applications. Wiley, Hoboken, NJ (2006)
104. The Basic Physics and Design of III-V Multijunction Solar Cells http://photochemistry.epfl.ch/EDEY/NREL.pdf. Accessed 6 Oct 2011
105. Walter, M.G., Warren, E.L., McKone, J.R., Boettcher, S.W., Mi, Q.X., Santori, E.A., Lewis, N.S.: Solar water splitting cells. Chem. Rev. **110**, 6446–6473 (2010)
106. Gibson, T.L., Kelly, N.A.: Predicting efficiency of solar powered hydrogen generation using photovoltaic-electrolysis devices. Int. J. Hydrogen Energy **35**, 900–911 (2010)
107. Ingler, W.B., Khan, S.U.M.: A self-driven p/n-Fe_2O_3 tandem photoelectrochemical cell for water splitting. Electrochem. Solid State Lett. **9**, G144–G146 (2006)
108. Miller, E.L., Rocheleau, R.E., Deng, X.M.: Design considerations for a hybrid amorphous silicon/photoelectrochemical multijunction cell for hydrogen production. Int. J. Hydrogen Energy **28**, 615–623 (2003)
109. Zhu, F., Hu, J., Kunrath, A., Matulionis, I., Marsen, B., Cole, B., Miller, E.L., Madan, A.: a-SiC:H films used as photoelectrodes in a hybrid, thin-film silicon photoelectrochemical (PEC) Cell for progress toward 10% solar-to hydrogen efficiency. Sol. Hydrogen Nanotechnol. Proc. SPIE **6650**, 66500S (2007)
110. Santato, C., Ulmann, M., Augustynski, J.: Photoelectrochemical properties of nanostructured tungsten trioxide films. J. Phys. Chem. B **105**, 936–940 (2001)

111. Arakawa, H., Shiraishi, C., Tatemoto, M., Kishida, H., Usui, D., Suma, A., Takamisawa, A., Yamaguchi, T.: Solar hydrogen production by tandem cell system composed of metal oxide semiconductor film photoelectrode and dye-sensitized solar cell. Proc. SPIE **6650**, 665003 (2007). doi:10.1117/12.773366
112. Hu, J., Zhu, F., Matulionis, I., Kunrath, A., Deutsch, T., Kuritzky, L., Miller, E.L., Madan, A.: Solar-to-hydrogen photovoltaic/photoelectrochemical devices using amorphous silicon carbide as the photoelectrode. 23rd European Photovoltaic Solar Energy Conference, Valencia, Spain, 1–5 September 2008
113. Matulionis, I., Zhu, F., Hu, J., Gallon, J., Kunrath, A., Miller, E.L., Marsen, B., Madan, A.: Development of a corrosion-resistant amorphous silicon carbide photoelectrode for solar-to-hydrogen photovoltaic/photoelectrochemical devices. SPIE Solar Energy and Hydrogen Conference, San Diego, USA, 10–14 August 2008
114. Stavrides, A., Kunrath, A., Hu, J., Treglio, R., Feldman, A., Marsen, B., Cole, B., Miller, E.L., Madan, A.: Use of amorphous silicon tandem junction solar cells for hydrogen production in a photoelectrochemical cell. SPIE Optics & Photonics Conference, San Diego, USA, 13–17 August 2006
115. Higashi, M., Abe, R., Ishikawa, A., Takata, T., Ohtani, B., Domen, K.: Z-scheme overall water splitting on modified-TaON photocatalysts under visible light ($\lambda < 500$ nm). Chem. Lett. **37**, 138–139 (2008)
116. Arakawa, H., Zou, Z., Sayama, K., Abe, R.: Direct water splitting by new oxide semiconductor photocatalysts under visible light irradiation. Pure Appl. Chem. **79**, 1917–1927 (2007)
117. Miller, E.L., Marsen, B., Cole, B., Lum, M.: Low-temperature reactively sputtered tungsten oxide films for solar-powered water splitting applications. Electrochem. Solid State Lett. **9**, G248–G250 (2006)
118. Yan, Y., Wei, S.-H.: Doping asymmetry in wide-bandgap semiconductors: origins and solutions. Phys. Stat. Sol. B **245**, 641 (2008)
119. Alexander, B.D., Kulesza, P.J., Rutkowska, I., Solarska, R., Augustynski, J.: Metal oxide photoanodes for solar hydrogen production. J. Mater. Chem. **18**, 2298–2303 (2008)
120. Cole, B., Marsen, B., Miller, E.L., Yan, Y., To, B., Jones, K., Al-Jassim, M.M.: Evaluation of nitrogen doping of tungsten oxide for photoelectrochemical water splitting. J. Phys. Chem. C **112**, 5213–5220 (2008)
121. Honga, S.J., Juna, H., Borsea, P.H., Lee, J.S.: Size effects of WO_3 nanocrystals for photooxidation of water in particulate suspension and photoelectrochemical film systems. Int. J. Hydrogen Energy **34**, 3234–3242 (2009)
122. Miller, E.L., Paluselli, D., Marsen, B., Rocheleau, R.E.: Low-temperature reactively sputtered iron oxide for thin film devices. Thin Solid Films **466**, 307–313 (2004)
123. Duret, A., Grätzel, M.: Visible light-induced water oxidation on mesoscopic α-Fe_2O_3 films made by ultrasonic spray pyrolysis. J. Phys. Chem. B **109**, 17184–17191 (2005)
124. Hu, Y.-S., Kleiman-Shwarsctein, A., Forman Hazen, A.J., Park, J.N., McFarland, E.W.: Pt-doped α-Fe_2O_3 thin films active for photoelectrochemical water splitting. Chem. Mater. **20**, 3803–3805 (2008)
125. Kleiman-Shwarsctein, A., Hu, Y.-S., Forman, A.J., Stucky, G.D., McFarland, E.W.: Electrodeposition of α-Fe_2O_3 Doped with Mo or Cr as Photoanodes for Photocatalytic Water Splitting. J. Phys. Chem. C **112**, 15900–15907 (2008)
126. Kay, A., Cesar, I., Grätzel, M.: New benchmark for water photooxidation by nanostructured α-Fe_2O_3 films. J. Am. Chem. Soc. **128**, 15714–15721 (2006)
127. Berglund, S.P., Flaherty, D.W., Hahn, N.T., Bard, A.J., Mullins, C.B.: Photoelectrochemical oxidation of water using nanostructured $BiVO_4$ films. J. Phys. Chem. C **115**, 3794–3802 (2011)
128. Liang, Y., Kleijn, S.J., Mooij, L.P.A., Van de Krol, R.: Defect properties and photoelectrochemical performance of $BiVO_4$ photoanodes. 216th ECS Meeting, Abstract #1172 (2009)

129. Enache, C.S., Lloyd, D., Damen, M.R., Schoonman, J., Van de Krol, R.: Photo-electrochemical properties of thin-film $InVO_4$ photoanodes: the role of deep donor state. J. Phys. Chem. C **113**, 19351–19360 (2009)
130. Chen, X., Liu, L., Yu, P.Y., Mao, S.S.: Increasing solar absorption for photocatalysis with black hydrogenated titanium dioxide nanocrystals. Science **331**, 746 (2011)
131. Yae, S., Kobayashi, T., Abe, M., Nasu, N., Fukumuro, N., Ogawa, S., Yoshida, N., Nonomura, S., Nakato, Y., Matsuda, H.: Solar to chemical conversion using metal nanoparticle modified microcrystalline silicon thin film photoelectrode. Solar Energy Mater. Solar Cells **91**, 224–229 (2007)
132. Sebastian, P.J., Mathews, N.R., Mathew, X., Pattabi, M., Turner, J.: Photoelectrochemical characterization of SiC. Int J. Hydrogen Energy **26**, 123–125 (2001)
133. Repins, I., Contreras, M.A., Egaas, B., DeHart, C., Scharf, J., Perkins, C.L., To, B., Noufi, R.: 19.9%-efficient ZnO/CdS/$CuInGaSe_2$ solar cell with 81.2% fill factor. Prog. Photovolt. Res. Appl. **16**, 235 (2008)
134. Bär, M., Weinhardt, L., Pookpanratana, S., Heske, C., Nishiwaki, S., Shafarman, W., Fuchs, O., Blum, M., Yang, W., Denlinger, J.D.: Depth-dependent band gap energies in Cu(In, Ga)(S, Se)2 thin films. Appl. Phys. Lett. **93**, 244103 (2008)
135. Bär, M., Bohne, W., Röhrich, J., Strub, E., Lindner, S., Lux-Steiner, M.C., Fischer, Ch-H: Determination of the band gap depth profile of the penternary $Cu(In_{(1-X)}Ga_X)(S_YSe_{(1-Y)})_2$ chalcopyrite from its composition gradient. J. Appl. Phys. **96**, 3857 (2004)
136. Bär, M., Weinhardt, L., Heske, C., Nishiwaki, S., Shafarman, W.: Chemical structures of the Cu(In, Ga)Se2/Mo and Cu(In, Ga)(S, Se)2/Mo interfaces. Phys. Rev. B **78**, 075404 (2008)
137. Marsen, B., Cole, B., Miller, E.L.: Photoelectrolysis of water using thin copper gallium diselenide electrodes. Solar Energy Mater. Solar Cells **92**, 1054–1058 (2008)
138. Jaramillo, T.F., Jørgensen, K.P., Bonde, J., Nielsen, J.H., Horch, S., Chorkendorff, I.: Identifying the active site: atomic-scale imaging and ambient reactivity of MoS_2 nanocatalysts. Science **317**, 100–102 (2007)
139. Maiolo, J.R.I.I.I., Atwater, H.A., Lewis, N.S.: Macroporous silicon as a model for silicon wire array solar cells. J. Phys. Chem. C **112**, 6194–6201 (2008)